Global and Planetary Change 237 (2024) 104462

Contents lists available at ScienceDirect

Global and Planetary Change

journal homepage: www.elsevier.com/locate/gloplacha

Uncovering Holocene climate fluctuations and ancient conifer populations: Insights from a high-resolution multi-proxy record from Northern Finland

J. Sakari Salonen [a,*], Niina Kuosmanen [a], Inger G. Alsos [b], Peter D. Heintzman [c,d], Dilli P. Rijal [b], Frederik Schenk [a,d,e], Freja Bogren [f], Miska Luoto [a], Annemarie Philip [g], Sanna Piilo [h], Liva Trasune [a], Minna Väliranta [h], Karin F. Helmens [i]

[a] Department of Geosciences and Geography, University of Helsinki, Helsinki, Finland
[b] The Arctic University Museum of Norway, UiT The Arctic University of Norway, Tromsø, Norway
[c] Centre for Palaeogenetics, Stockholm, Sweden
[d] Department of Geological Sciences, Stockholm University, Stockholm, Sweden
[e] Bolin Centre for Climate Research, Stockholm University, Stockholm, Sweden
[f] Department of Physical Geography, Stockholm University, Stockholm, Sweden
[g] Institute for Biodiversity and Ecosystem Dynamics, University of Amsterdam, Amsterdam, the Netherlands
[h] Ecosystems and Environment Research Programme, University of Helsinki, Helsinki, Finland
[i] Swedish Museum of Natural History, Stockholm, Sweden

ARTICLE INFO

Editor: Dr. Jed O Kaplan

Original content:
Salonen_ea-Kuutsjarvi-Supplementary_data.xlsx (Original data)

Keywords:
Ellenberg indicator values
Summer temperature
Moisture
CESM1
Atlantic meridional overturning circulation
*seda*DNA

ABSTRACT

A series of abrupt climate events linked to circum-North Atlantic meltwater forcing have been recognised in Holocene paleoclimate data. To address the paucity of proxy records able to characterise robustly the regional impacts of these events, we retrieved a sub-centennial resolution, well-dated core sequence from Lake Kuutsjärvi, northeast Finland. By analysing a range of paleo-environmental proxies (pollen, plant sedimentary ancient DNA, plant macrofossils, conifer stomata, and non-pollen palynomorphs), and supported with proxy-based paleo-temperature and moisture reconstructions, we unravel a well-defined sequence of vegetation and climate dynamics over the early-to-middle Holocene. The birch-dominated pioneer vegetation stage was intersected by two transient tree-cover decrease events at 10.4 and 10.1 thousand years ago (ka), likely representing a two-pronged signal of the 10.3 ka climate event. Our data also show a clear signal of the 8.2 ka climate event, previously not well recorded in the European Arctic, with a collapse of the pine-birch forest and replacement by juniper developing in tight synchrony with Greenland isotopic proxies over 8.4–8.0 ka. Supported by climate modelling, severe winter cooling rather than summer might have been driving vegetation disruptions in the early Holocene. The Kuutsjärvi data indicate an early arrival of Norway spruce (*Picea abies*) by 9.2 ka (pollen, DNA, and stoma finds), as well as the first evidence for Holocene presence of larch (*Larix*) in Finland, with pollen finds dating to 9.6–5.9 ka.

1. Introduction

Widespread proxy data indicate repeated abrupt, sub-millennial disruptions in Northern Hemisphere climate in the early part of the current interglacial (12–8 ka), commonly linked to climatic and oceanic impacts of freshwater routing and outburst floods related to the residual ice sheets in North America and Europe (Bond et al., 1997; Clark et al., 2001). In continents surrounding the North Atlantic, the best-documented Holocene centennial event is the 8.2k event, named after its estimated age at 8.2 ka. The 8.2k event has been associated with a range of environmental impacts, including cooling and drying in Europe, Greenland and eastern North America (Alley and Ágústsdóttir, 2005). However, indications of North Atlantic freshwater forcing and widespread cooling have also been documented at 9.3 ka and 10.3 ka as well as during the Preboreal Oscillation (11.4 ka) of the first centuries of the Holocene (Björck et al., 1997; Björck et al., 2001; Bond et al., 1997; Clark et al., 2001; Rasmussen et al., 2007). In Europe, early-Holocene abrupt cooling events have also been associated with minima in archaeological datings, suggesting a possible influence on ancient human populations as well (Herrle et al., 2018; Tallavaara et al., 2014).

* Corresponding author.
E-mail address: sakari.salonen@helsinki.fi (J.S. Salonen).

https://doi.org/10.1016/j.gloplacha.2024.104462
Received 11 October 2023; Received in revised form 30 April 2024; Accepted 6 May 2024
Available online 8 May 2024

However, the precise climate signals of these abrupt events remain poorly resolved, including the amplitude and seasonality of associated temperature and moisture changes, as well as spatial expression and possible inter-regional correlations. This is due to the paucity of high-resolution proxy datasets, as well as seasonal biases in the available proxies (Kaufman et al., 2020a; Salonen et al., 2012; Salonen et al., 2019; Sundqvist et al., 2010), hampering a consistent hemispheric detection and characterization of the events. Due to their linkage to North Atlantic freshwater forcing, there is a growing interest to leverage the late-Quaternary abrupt events and explore the climatic impact of possible future disturbance in ocean circulation due to glacier melt (Alley and Ágústsdóttir, 2005; Schenk and Wohlfarth, 2019), underlining the need for an expansive network of high-resolution, multiproxy datasets describing the variation of seasonal temperature and precipitation during past abrupt events.

In this study, we describe the high-resolution and robustly-dated sediment core from lake Kuutsjärvi, NE Finland (Fig. 1), recording a series of abrupt early-Holocene vegetation shifts and sub-millennial climate events in the European Arctic. The Kuutsjärvi sequence has been analysed for a range of fossil proxies including pollen data with sub-centennial (~ 50 year) resolution through the early and middle Holocene, complemented by records of plant macrofossils, conifer stomata, and non-pollen palynomorphs (NPPs). In addition to the classical fossil proxies, we present a high-resolution record of sedimentary ancient DNA (*sed*aDNA) which has in recent studies proven a powerful complement to fossil proxies in unravelling past biotic and abiotic changes (Bjune et al., 2022; Brown et al., 2022; Garcés-Pastor et al., 2022). To quantify past climatic conditions, we prepare a high-resolution reconstruction of Holocene climate using an ensemble of pollen–July temperature (T_{jul}) calibration models (Salonen et al., 2018; Salonen et al., 2019), supported by vegetation community level estimates of climatic requirements (Ellenberg indicator values; Tyler et al., 2021) calculated from both pollen and *sed*aDNA samples. Finally, we incorporate high-resolution climate simulations for the early Holocene to evaluate hypotheses about potentially limiting climate parameters that may explain ecological responses to abrupt events revealed by the Kuutsjärvi proxy data.

2. Methods

2.1. Site and coring

Lake Kuutsjärvi (67°44′49″N 29°36′36″E, 341 m a.s.l.) is located in the Värriö Strict Nature Reserve in NE Finland (Fig. 1A), adjacent to the Värriö Research Station of the University of Helsinki. The lake (Fig. 1B) is situated in a sheltered position at the head of a canyon, cut by Fennoscandian Ice Sheet meltwaters into the northern slope of the first mountain (Ykkönen) in the Värriötunturit chain of low mountains. Kuutsjärvi measures approximately 135 m in length, 75 m in width, and 0.65 ha in surface area, and has a very small catchment of <2 km^2. The lake bathymetry (Fig. 1C) was mapped with sonar (Humminbird 797c2i) from 361 locations using a boat. Water depth (ca. 8 m) and sediment thickness (ca. 6 m) are greatest in the western portion of the lake near its apex, and it is here that the sediment coring boreholes were located. Presently, the lake is fed by a small rivulet (inlet) in the NW. The water depth at the outlet in the NE is ca. 1 m, but significantly more during spring melt and probably less in the summer. The lake is ice-covered from October to late May or early June. The south-facing steep slope along the lake is dry and dominated by pine (*Pinus sylvestris*). The north-facing steep slope, and the flat bottom of the canyon at the lake outlet, are dominated by spruce (*Picea abies*). Abundant *Salix*, *Equisetum* and *Chamaepericlymenun suecicum* further characterise the latter swamp forest. The lake shore is dominated by *Salix* spp., *Carex*, *Comarum palustre* and *Sphagnum* fringed by alternating narrow belts of *Carex* and *Equisetum.* The lake inlet is surrounded by a mixed forest with tall forbs (*Filipendula ulmaria, Chamaenerion angustifolium*), ferns (*Phegopteris connectilis, Gymnocarpum dryopteris*) and patches of wetland dominated by *Comarum palustre*. Furthermore, dwarf shrubs (*Vaccinium vitis-idaea, V. myrtillus, V. uligonosum, Empetrum nigrum, Rhododendron tomentosum*) are common throughout the catchment.

Kuutsjärvi was cored in April 2016 (Fig. 1C) using a heavy PP-piston corer (Putkinen and Saarelainen, 1998) with a diameter of 6 cm. Two

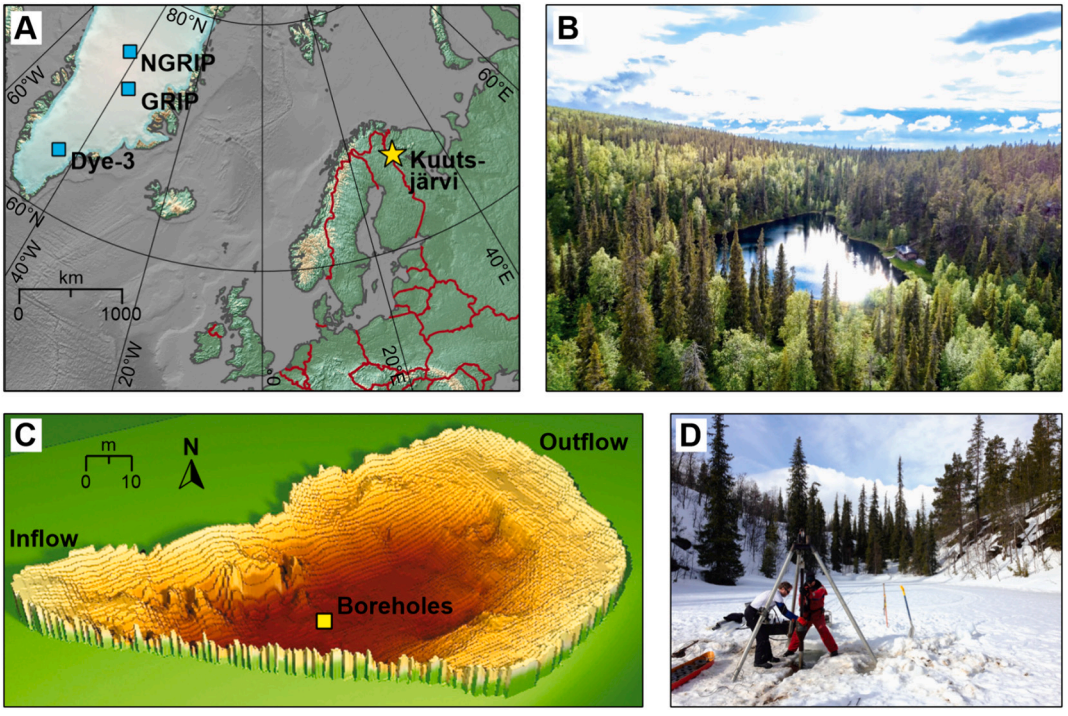

Fig. 1. (A) Location of Kuutsjärvi in Finland (*star*) and supporting data sites in Greenland (*squares*); (B) Aerial view westward over of Kuutsjärvi in summer; (C) Sonar bathymetry of Kuutsjärvi with the coring site indicated; (D) Coring at Kuutsjärvi in April 2016.

parallel sequences (KJ1 and KJ2, at ca. 1 m distance from each other), were obtained in overlapping 2-m long core sections and with a total sediment core length of ca. 5.9 m. The KJ1 sequence was used for radiocarbon dating and most proxy analyses described in this paper (pollen, plant macrofossils, loss on ignition; see below) while the subsamples for *sed*aDNA analysis were taken from KJ2. Some of the *sed*aDNA results from Kuutsjärvi have been published before in Rijal et al. (2021), while this paper adds both additional *sed*aDNA samples and a revised chronology based on additional radiocarbon dates compared to Rijal et al. (2021).

2.2. Dating and chronology

A chronology for Lake Kuutsjärvi was created from 23 radiocarbon samples, of which 19 have been published earlier (Rijal et al., 2021) and four supplementary dates were added here from 39, 59, 63, 73 cm depth (Table S1). Age-depth modelling was done with the Bayesian algorithm Bacon (Blaauw and Christen, 2011), using the rbacon library (Blaauw et al., 2022) for R (R Core Team, 2022), with the default segment length of 5 cm, accumulation shape of 3, and the default accumulation rate of 20.

In addition to the 540 cm thick gyttja spanned by the age-depth model, our proxy data include pollen and plant macrofossil samples from an underlying, ca. 50 cm thick organic-bearing minerogenic layer that is interpreted to represent a brief time interval. This minerogenic bottom layer was deposited in a series of overflow events when meltwater from the Fennoscandian Ice Sheet overtopped a nearby col. in the Värriö mountain ridge, <0.5 km west from Kuutsjärvi lake (Bogren, 2019). According to the deglaciation chronology of NE Finland (Johansson, 1995; Johansson, 2007), the deglaciation of the area between Kuutsjärvi in the east and the Nuortti canyon some 15 km to the west lasted less than ~100 years. Bogren (2019) estimates that the ice was in position to produce the overflow events into the Kuutsjärvi basin for approximately 10 years, and hence the minerogenic deposits at the base of the Kuutsjärvi sequence are estimated to represent at most ~10 years of sedimentation.

2.3. Pollen analysis

Pollen samples were prepared from 1 cm^3 subsamples, using HCl, KOH, sieving (212 μm mesh), acetolysis, and bromoform heavy-liquid treatments, and mounted in glycerol. A total of 167 pollen samples were counted, mostly at 2 or 4 cm intervals, with a mean of 517 (min = 339, max = 784) terrestrial pollen and spore grains counted from each sample. The pollen sampling resolution is sub-centennial across the early- and middle-Holocene with a mean age gap of 47.1 years between samples (min = 17 years, max = 80 years) through the 10.6–4.0 ka interval. Due to the shift to a slower sedimentation, between 4 and 0 ka the mean age gap increases to 159.7 years (min = 66 years, max = 332 years). The pollen counts were increased above 700 in the late-Holocene sections with the largest age gaps, as the larger counts result in smaller random variations in the pollen percentage values (Maher, 1972), providing an alternative strategy to stabilise the pollen-based climate reconstruction when increasing the temporal resolution is not possible. Conifer stomata, charcoal (with a minimum size cutoff of a small pollen grain, ~20 μm), *Lycopodium* marker grains (Stockmarr, 1971), and non-pollen palynomorphs were also counted from the pollen slides. Pollen and spores were identified according to Moore et al. (1991) and Reille (1992) and stomata according to Sweeney (2004).

2.4. Plant macrofossil analysis

Plant macrofossil samples were prepared at 1–5 cm intervals from subsamples of mainly ca. 5 cm^3. The subsamples were sieved using a 100-μm mesh and the residue was examined under a stereomicroscope and high-magnification light microscopes. No chemical treatment was necessary. All remains were counted and identified to the lowest possible taxonomic level, mainly based on Mauquoy and van Geel (2013) and Birks (2013).

2.5. Sedimentary ancient DNA (sedaDNA) analyses

Sedimentary ancient DNA data were generated from subsamples taken from core KJ2, as previously described in Rijal et al. (2021). We supplemented an existing dataset, derived from 45 subsamples from Rijal et al. (2021) and Alsos et al. (2022), with 15 new subsamples for a total of 60 *sed*aDNA samples from Kuutsjärvi. One *sed*aDNA sample (EG21_TS540) was excluded, as it fell outside of the age-depth model, and so a total of 59 samples were used for the final analyses. We also generated data from nine new controls to give 17 controls in total, and re-extracted two samples from around the 8.2 ka event (EG21_L362a and EG21_L378a) (Supplementary Data). For the newly generated data, we extracted, amplified, and sequenced *sed*aDNA using the same plant metabarcoding approach as in Rijal et al. (2021), but with refined taxonomic assignments using the PhyloNorway reference database, following Alsos et al. (2022). All new raw sequencing data have been deposited in the European Nucleotide Archive (project PRJEB39329), with the primer tag-to-sample lookup file provided in the Supplementary Data. For the previously published *sed*aDNA subsamples, ages had been derived from an earlier age-depth model that was inferred by correlating the KJ1 and KJ2 sediment cores, as radiocarbon dates were derived from KJ1 and the *sed*aDNA samples were taken from KJ2. Here, we revised all *sed*aDNA sample ages based on an updated correlation between the KJ1 and KJ2 cores and the updated age-depth model which is presented and used for all proxies in this study. Using these revised ages, the mean sampling resolution for our *sed*aDNA samples was 180 years (sd = ± 173 years, min = 5 years, max = 1004 years). Only three late-Holocene samples were separated by a > 500-year gap. The early-, middle-, and late-Holocene samples had mean age gaps of 177 (± 104), 125 (± 58), and 306 (± 313) years respectively. The 13 negative controls used to monitor for contamination in the ancient DNA lab contained sporadic detections of *Alnus incana*, *Picea abies*, *Rhodobryum roseum*, each occurring in only 1/104 of the total polymerase chain reaction (PCR) repeats, and *Angelica archangelica*, which occurred in 2/104 PCR repeats (Supplementary Data).

2.6. Data analyses of proxy records

A constrained cluster analysis with Bray-Curtis distance was performed using the incremental sum of squares (CONISS) (Grimm, 1987) approach, applied separately on terrestrial plant data based on *sed*aDNA PCR repeats and on pollen, to define compositional change boundaries. Pollen counts and PCR repeats were converted proportions prior to cluster analysis. Broken stick models were used to select a statistically significant number of vegetation clusters.

To estimate taxonomic richness in each proxy record, we used the total number of taxa detected in each sample as a measure of richness for *sed*aDNA and plant macrofossils, while rarefied pollen richness (Birks and Line, 1992) was used for pollen calculated based on the sample pollen sum. Temporal trends in richness were visualised using generalised additive models (GAM) following Rijal et al. (2021).

Rates of change through the pollen sequence were estimated with detrended correspondence analysis (DCA) performed on the terrestrial pollen data (implemented using the vegan library for R; Oksanen, 2022). The rates of change were calculated as Euclidean distances of DCA the sample values (using the first two DCA components) between adjacent pollen samples, divided by the sample age gaps (Correa-Metrio et al., 2014).

2.7. Paleoclimate reconstructions

A pollen-based paleoclimate reconstruction was prepared using an

ensemble of six pollen–T_{jul} calibration models. This ensemble has earlier been employed with the last interglacial (LIG) sequence from nearby Sokli and is discussed in detail in Salonen et al. (2018); further discussion on the calibration data and validation of calibration models is also found in Salonen et al. (2019). The calibration models used include three classical, unimodal transfer functions, the weighted averaging (WA; Birks et al., 1990), weighted averaging-partial least squares (WA-PLS; ter Braak and Juggins, 1993), and maximum likelihood regression curves (MLRC; Birks et al., 1990). Also used were the modern analogue technique (MAT; Overpeck et al., 1985) as well as two machine-learning methods based on ensemble models of regression trees, the random forest (RF; Breiman, 2001) and the boosted regression tree (BRT; De'ath, 2007). The reconstruction errors of the models, estimated as the root-mean-square error of prediction in ten-fold cross-validations, range from 1.12 to 2.05 °C (Salonen et al., 2018). The calibration models were prepared in R using the libraries GBM (Ridgeway, 2020), RANDOMFOREST (Liaw and Wiener, 2002), and RIOJA (Juggins, 2020). The reconstructions are synthesised as a median of the T_{jul} curves produced by the six models, as well as a LOWESS smoother (span 0.05, one robustifying iteration) fitted to the median. A 95% error band was produced by calculating the median curve 1000 times from bootstrap samples of all six reconstructions and extracting the 2.5th and 97.5th percentiles.

2.8. Reconstruction of plant ecological indicator values

To aid in the assessment of the possible climatic factors that may have caused the variations in our proxy data, we complemented our pollen-based T_{jul} reconstruction with reconstruction of selected ecological indicator values of plants, including the so-called Ellenberg values for moisture requirement and temperature optimum (Tyler et al., 2021), from our pollen and *sed*aDNA data. With pollen, we first calculated a moisture requirement value for each tree and shrub pollen type, as the mean moisture requirement value of all species included in that pollen type (Tyler et al., 2021). A Holocene moisture requirement curve was then prepared by calculating for each fossil sample the mean of the pollen type-specific indicator values, weighted by pollen abundance. For each *sed*aDNA sample, we calculated the proportion of PCR repeats, a conservative quantitative proxy for plant abundance, of each indicator value category for both temperature optimum and moisture requirement, following the methodology of Alsos et al. (2022) and using the same Tyler et al. (2021) indicator value data as above. Temperature optimum was expressed on an 18-category scale ranging from 1 (subtropical) to 18 (high arctic-alpine) with the current data representing categories 5–16. Moisture requirement ranges from 1 (very dry) to 12 (deep permanent water), but we only included plants from the terrestrial range (2–9; no taxa with the value 1 were recorded) for the plots tracking the moisture variation through time.

2.9. Analysis of plant climatic tolerances

To constrain the possible winter temperature regime in the early Holocene, we estimated the cold tolerance of mountain birch (*Betula pubescens* subsp. *tortuosa*). Utilizing the predominant Eurasian distribution data of *Betula pubescens* (observations for *Betula pubescens* subsp. *tortuosa* are geographically limited to Fennoscandia), as sourced from GBIF (Global Biodiversity Information Facility) and complemented by CHELSA (Climatologies at High resolution for the Earth's Land Surface Areas) climate data spanning the period 1981–2010, a temperature limit of the species can be estimated: the contemporary average temperature during the coldest month within the species' coldest distributed sites situated in the northern expanse of Siberia was determined to be −35.9 °C. The corresponding value based on the observation of *Betula pubescens* subsp. *tortuosa* was only −13.9 °C, which is possibly an overly conservative estimate. We assume that the majority of the GBIF observations at the coldest sites with *Betula pubescens* actually represent *Betula pubescens* subsp. *tortuosa*. The species' tolerance with regard to minimum temperature was determined based on the coldest observed range of the species using January mean temperature data.

2.10. Paleoclimate model simulations

To put paleoclimate reconstructions and paleo-environmental changes in the early Holocene into a broad-scale physical-dynamical context, the results are compared to simulated changes in January and July temperature relative to the pre-industrial (1850 CE) average. High-resolution (0.9° × 1.25°) global climate simulations were performed as snapshot simulations of climate states for 11 and 9 ka with the Community Earth System Model (CESM1.0.5) using the same model setup as for an earlier set of simulations for the deglaciation (Kuang et al., 2021; Schenk et al., 2018). Horizontal boundary conditions for sea-surface temperatures (SST) and sea-ice (ice fraction) were prescribed in our simulation with a climatology based on the monthly means over ±50 years centred around 11 and 9 ka derived from a previous fully-coupled transient atmosphere-ocean simulation conducted for the last 22 ka years at a coarser model resolution (He et al., 2013; Liu et al., 2009). The paleo-topography was adjusted to past sea-level lowstands and continental ice sheets are included in CESM1 together with setting orbital forcing parameters to 11 and 9 ka as well as prescribing greenhouse gas concentrations as ±50 year averages around 11 and 9 ka, respectively. In addition to surface temperature anomalies, mean near-surface wind patterns from the lowest model level (sigma 992 hPa) for past climate states are shown highlighting the dominating wind pattern across northern Europe.

3. Results

3.1. Chronology

The chronology of Kuutsjärvi is based on 23 radiocarbon dates prepared from macrofossil fragments of terrestrial plants (Table S1). The fitted age–depth model (Fig. 2) spans the 540 cm thick gyttja deposit, indicating a bottom age for continuous biogenic sedimentation at ~10.6 ka. A stable sedimentation rate and a relatively tight error band (mean 95% range = 308 years) is indicated from the bottom to approximately 3.8 ka, followed by a shift to a considerably slower sedimentation and larger modelled age errors from 3.8 ka to core top (mean 95% range = 455 years).

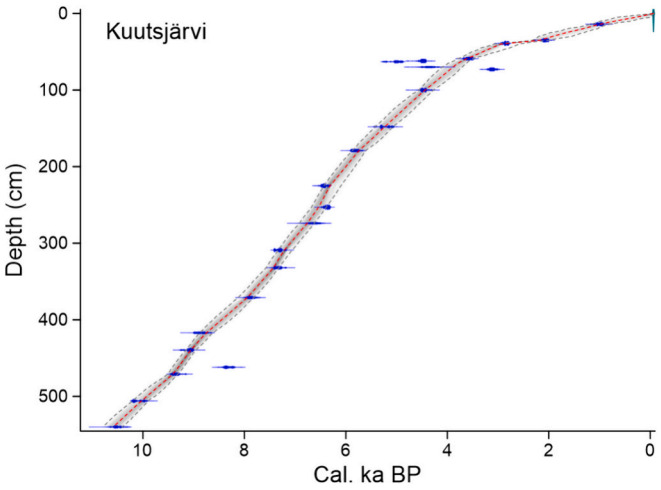

Fig. 2. Kuutsjärvi age–depth model, including the median age estimate (*red dashed line*) and the 95% error margins (*grey dashed lines*). The calibrated age distributions of the underlying radiocarbon dates ($N = 23$) are indicated in *blue*. (For interpretation of the references to colour in this figure legend, the reader is referred to the web version of this article.)

3.2. Taxonomic richness detected

For *sed*aDNA, a total of 12,095,031 raw reads were obtained for 62 samples (including two extraction duplicates), of which we retained 5,821,240 reads after quality filtering. The *sed*aDNA dataset recorded 156 plant taxa of which 49% and 23% were identified to the species and genus levels, respectively.

For pollen, 63 taxa were identified in 167 samples of which 33% and and 41% were identified to the species and genus level, respectively. Over a half of the species-level identifications for pollen (11 out of 21) were achieved implicitly, i.e., as identifications of a genus with only one species occurring in Fennoscandia. Six taxa are assumed to be of extrazonal origin, consisting of small amounts of thermophile tree pollen.

An increase in taxonomic richness is seen throughout the Holocene for both pollen and *sed*aDNA, but this increase is much steeper in *sed*aDNA than pollen, with *sed*aDNA richness expanding from fewer than 10 taxa per sample to >60, whereas pollen richness increases from 19 to on average 24 taxa per sample (Fig. 3). The proportion of different growth forms remains rather stable through the period in the pollen data, which are dominated by trees and shrubs followed by vascular cryptogams and graminoids. In the *sed*aDNA record, trees and shrubs are co-dominant with forbs, with lower abundance of vascular cryptogams, dwarf shrubs, aquatics and bryophytes (Fig. 4). There is also a clear shift in growth form over time, with especially dwarf shrubs and aquatics increasing from about 9.2 ka. We note that graminoids are poorly represented in the *sed*aDNA record before 9.2 ka, whereas their proportion in pollen is quite stable throughout the period.

For plant macrofossils, the taxonomic diversity was overall lower, however varying greatly through the sequence. The uppermost 80% of the sequence yielded an overall low density of finds, and, particularly in the gyttja below 450 cm sediment depth (age > ~9.1 ka), only few and largely broken macrofossils were found. However, in the lowermost minerogenic sediment underlying the gyttja, the macrofossil record is considerably richer. In total, 34 taxa were detected in 56 macrofossil samples of which 15 (44%) and 13 (38%) were identified to species and genus level, respectively.

3.3. Vegetation changes

The CONISS analyses show that major changes in composition are detected at about the same time in *sed*aDNA and pollen, at 9.3–9.2, 7.4–7.35 and 6.2–6.0 ka, whereas the most recent change is earlier in *sed*aDNA (4.4 ka) than pollen (3.2 ka) (Figs. S1–S2). Here, we adopt a zonation using the the three oldest splits indicated by both *sed*aDNA and pollen (9.3, 7.3, and 6.2 ka), while for the last split we favour the earlier timing indicated by *sed*aDNA (4.4 ka), due to the higher taxon diversity of *sed*aDNA compared to pollen (Fig. 3). This results in five biostratigraphic zones (designated I to V).

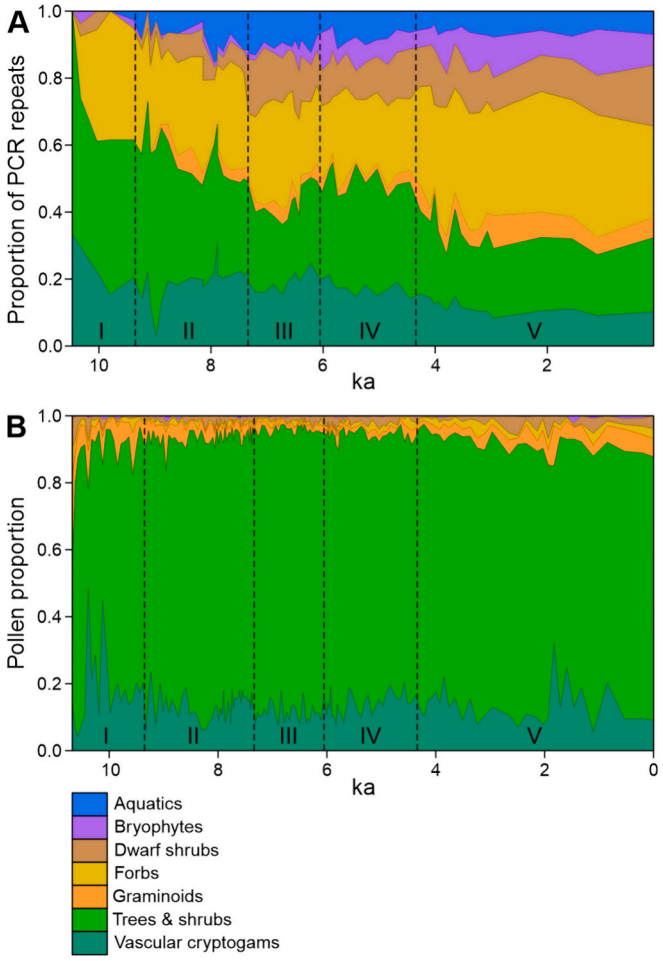

Fig. 4. Proportion of *sed*aDNA PCR repeats and pollen for different plant growth forms in the Kuutsjärvi sequence. Biostratigraphic zones identified based on pollen and/or *sed*aDNA based CONISS zonations are indicated with Roman numerals.

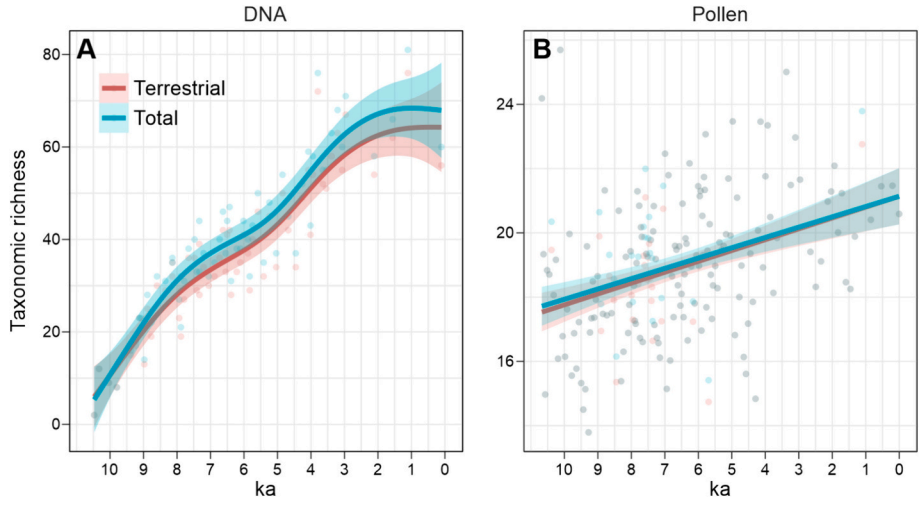

Fig. 3. Total and terrestrial richness of taxa detected in (A) *sed*aDNA and (B) pollen in the Kuutsjärvi sequence. Note the difference in y-axis scales.

3.3.1. Zone I: 10.6–9.3 ka (samples: 6 sedaDNA, 23 pollen, 20 macrofossil)

All three proxies show that trees are already present in the earliest samples (Fig. 5A). During the first millennium, the Kuutsjärvi pollen sequence is dominated by *Betula pubescens/pendula* (Fig. 3). The sub-arctic birch forest, presumably composed of mountain birch (*B. pubescens* subsp. *tortuosa*), already established itself at the site in the ice-marginal environment, with tree-type birch pollen reaching 70% and seeds present in the basal minerogenic sediment. The macrofossil record from the gyttja deposit is relatively scarce, and limited *Betula sed*aDNA was extracted from the lower part of Zone I (Fig. 3). However, abundant tree-type *Betula* seeds are encountered in Loitsana lake, located some 10 km west of Kuutsjärvi, throughout the early-Holocene birch forest stage (Shala et al., 2014).

In contrast to the scarce macrofossil record from the Kuutsjärvi gyttja, a rich macrofossil plant assemblage has been retrieved from the basal glacio-fluvial sediment (Fig. 5 and Fig. S6). In addition to tree birch, it records the presence of various shrubs (e.g. *B. nana*, *Empetrum nigrum*, *Vaccinium vitis-idaea*, *Calluna vulgaris*), a rich herb flora including the arctic-alpine species *Dryas octopetala* and *Saxifraga* cf. *cernua*, bryophytes (e.g., *Polytrichum jensenii*, *P. strictum*) and ferns (fern sporangia present).

Scattered occurrences of *Pinus* and *Populus* are found in both DNA and pollen. A low percentage of Ericaceae pollen is found along with scattered occurrences of *Vaccinium uliginosum* and *V. vitis-idaea sed*aDNA. A rich cryptogram record and only scattered aquatics are found in both DNA and pollen (Fig. 4). Similarly, based on DNA, *Urtica dioica* was among the first arrivals.

Within the *Betula* stage, two pollen turnover spikes consisting of strong tree pollen minima are recorded at 10.4 and 10.1 ka (Fig. 5A). These tree-cover decrease events are composed of 65% and 50% reductions, respectively, in tree-type *Betula* pollen, with corresponding pollen maxima in dwarf birch (*B. nana*) (Fig. 5A) and willow (*Salix*) (Fig. 5B) shrubs and total herbs (Fig. 5A), and also align with maxima of the coprophilous fungal spore sum (including the *Cercophora, Podospora*, and *Sporormiella* types; van Geel, 2001) and charcoal (Fig. 5B). Similar changes are not observed in the *sed*aDNA record, where the closest sampling dates are 10.1 and 10.3 ka.

Over 9.4–9.3 ka birch pollen is sharply replaced by pine pollen (*Pinus*) as the dominant tree. At the same time, *Pinus* stomata become nearly continuously recorded, macrofossils (e.g. needles) are found, and *Pinus* becomes consistently detected in *sed*aDNA, indicating the establishment of pine forest.

3.3.2. Zone II: 9.2–7.4 ka (samples: 16 sedaDNA, 47 pollen, 10 macrofossil)

Zone II shows sporadic occurrences of larch (*Larix*) pollen grains (Fig. 6A–E), with the earliest find recorded at 9.6 ka. Meanwhile, a transient early-Holocene occurrence of *Picea* is indicated by pollen as well as *sed*aDNA (Fig. 5A), and with a *Picea* stoma indicating the deposition of a needle in the sediment and thus local presence. The stoma find (Fig. 6F), dating to 8.9–8.7 ka, is robustly identifiable as *Picea* (and not *Pinus*) based on the stoma width to stem width ratio of >7 and thin medial lamellae borders (Sweeney, 2004).

A sudden tree pollen minimum, driven by a strong *Juniperus* pollen peak and also associated with a peak in *J. communis sed*aDNA, occurs at 8.4–8.0 ka, which aligns well with the 8.2k cooling event (Alley and Ágústsdóttir, 2005; Alley et al., 1997). The abrupt decline of *Juniperus* and rise of the tree curve at the end of the event at 8.0 ka marks the fastest pollen turnover of the Holocene at Kuutsjärvi. The *sed*aDNA peak of *Juniperus* at 8.1 ka was replicated using two DNA extractions, resulting in 5/8 and 6/8 PCR repeats detecting *Juniperus*, but was undetected in adjacent samples at 8.4 and 7.9 ka.

The number of taxa detected in *sed*aDNA almost doubles in Zone II (Fig. 3), with numerous graminoids, forbs, aquatics, and cryptograms arriving (Figs. 4 and 5B). Many detected taxa benefit from nutrient/nitrogen-rich conditions, such as *Urtica dioica* and *Chamaenerion angustifolium*, the latter effectively acting as a pioneering taxon occupying new terrain.

3.3.3. Zone III: 7.3–6.1 ka (samples: 12 sedaDNA, 32 pollen, 9 macrofossil)

Following the 8.2 ka event, total tree pollen starts a gradual rise lasting until ca. 7.3 ka, reaching Holocene maximum levels of 90–95% which last until 4 ka. Thermophile tree pollen (*Ulmus*, *Corylus*, *Quercus*, *Fraxinus*, *Tilia*, and *Carpinus*, in decreasing order by total pollen count), judged to be entirely long-distance transported, reaches its maximum at ~0.7% through Zones III and IV (Fig. 5A). Both *sed*aDNA and pollen show a decrease in *Salix* for this period (Fig. 5B), whereas the tree taxa remain at similar levels as in the previous period. *Vaccinium myrtillus* appears and contributes to the overall increase in dwarf-shrub abundance in *sed*aDNA (Fig. 4) while only a minor increase is seen in Ericaceae pollen. We note a sharp disappearance of *Sparganium* in pollen while it still persists in *sed*aDNA.

3.3.4. Zone IV: 6.0–4.4 ka (samples: 12 sedaDNA, 35 pollen, 6 macrofossil)

There is a rise in pollen turnover at 6 ka, associated with a sharp increase in *Alnus* pollen from 6.0 ka, when it also appears in all PCR repeats in almost every sample, suggesting that it is common in the catchment from this time. This major vegetation transition is immediately followed by the last find of *Larix* pollen at 5.9 ka. *Diplazium sibiricum* disappears from the *sed*aDNA record, whereas several new forbs appear (Fig. 4) including *Actaea spicata* (Fig. 5B) and multiple species of *Ranunculus* (Fig. S4).

3.3.5. Zone V: 4.3–present (samples: 15 sedaDNA, 30 pollen, 11 macrofossil)

In pollen, the total tree and *Alnus* curves fall, whereas *Picea* rises (Fig. 5A). There is an increase in *Juniperus communis sed*aDNA and *Juniperus* pollen, as well as an overall increase in shrub and herb pollen. The *sed*aDNA data show an increase in shrub taxa including *Empetrum nigrum, Arctostaphylos uva-ursi*, and *Pyrola*, as well as the *Linnaea borealis* sub-shrub. Many new taxa of bryophytes appear (Fig. 4) while large ferns either decrease (*Mattheucia*) or disappear (*Athyrium distentifolium*) (Fig. 5B). Forbs occur at high abundance in *sed*aDNA whereas ferns reach their lowest abundance (Fig. 4). Overall, this suggests a shift from tall-forb forest to dwarf-shrub forest. From 3 ka onward, *Myriophyllum* appears in both pollen and *sed*aDNA whereas *Hippuris* becomes rare in *sed*aDNA (Fig. 5B), suggesting some changes in aquatic conditions.

3.4. Climate reconstructions

The pollen-based T_{jul} reconstruction from Kuutsjärvi is shown in Fig. 7B. The last interglacial (LIG) reconstruction from the Sokli site (discussed in detail in Salonen et al. (2018)), located ca. 15 km to the northwest and using the same reconstruction method, is shown for comparison in Fig. 7A.

The early part of the Holocene reconstruction (10.6–9.3 ka) is characterised by a large spread of the calibration model ensemble, ranging from ca. 2 °C below present day values to 0–1 °C above present. These fossil samples also show the largest compositional distances (grey silhouette curves in Fig. 7) between the fossil samples and the modern calibration samples, indicating that poor modern analogues are found for the fossil samples of Zone I, which is rich in tree-type *Betula* (Fig. 5A). Starting from 9.3 ka, and the onset of the *Pinus*-dominated zone, the reconstruction ensemble converges to indicate T_{jul} of ca. 0–1 °C above present. This warm period is interrupted by a strong cooling event spanning seven pollen samples over 8.4–8.0 ka, with the ensemble median showing a gradual T_{jul} fall of ca. 2 °C culminating at 8.1 ka and followed by a more rapid recovery over ca. 100 years. The 8.4–8.0 ka event is followed by a steady rise of temperature, culminating in a

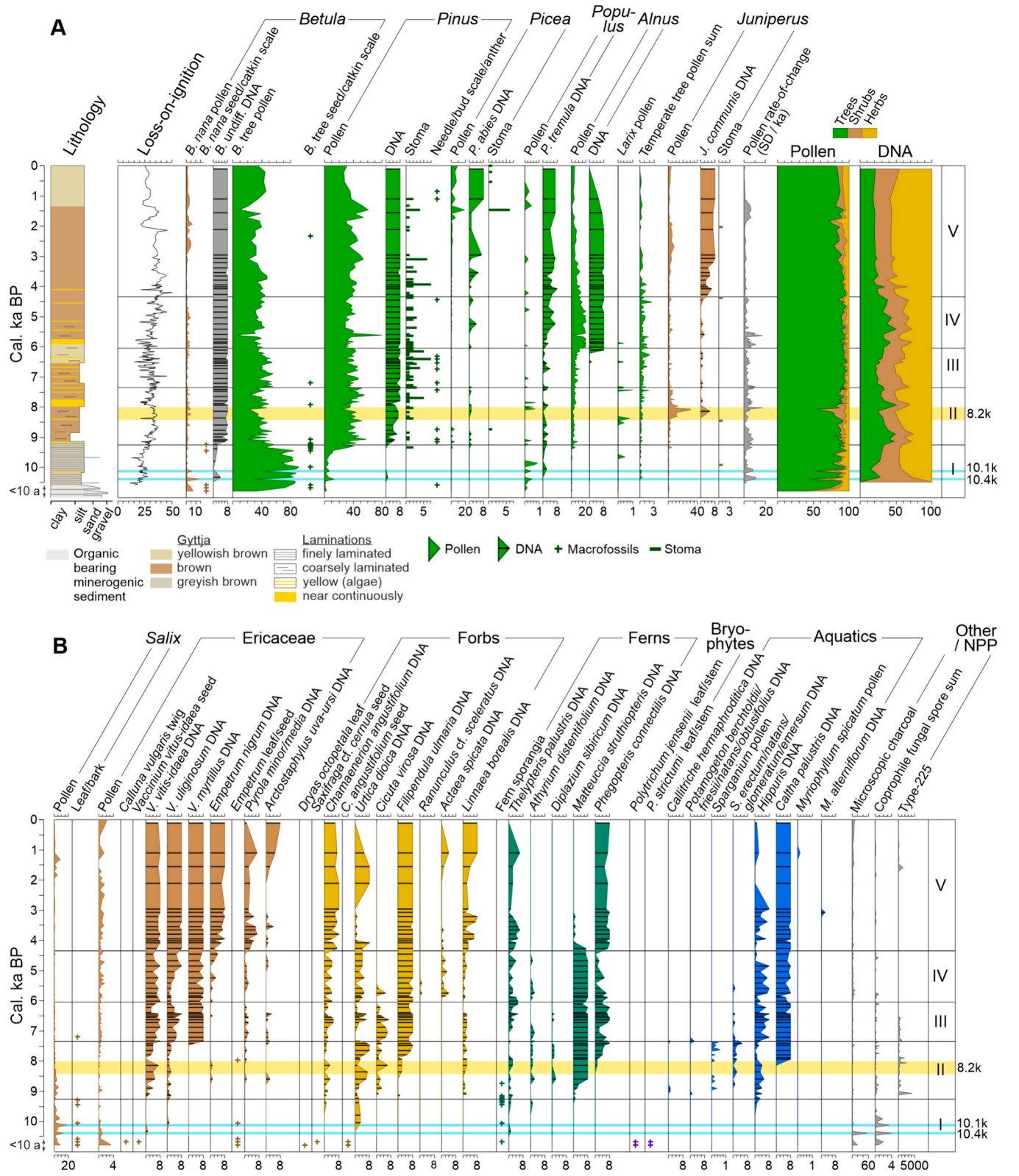

Fig. 5. Summary of the Kuutsjärvi multiproxy dataset. (A) Lithology and key terrestrial vegetation components summarised from pollen, *sed*aDNA, macrofossil and stomatal data. (B) Data for selected plant indicator species, charcoal, and selected non-pollen palynomorphs (NPPs). For the full data, see Figs. S3–S6 and Supplementary Data. Biostratigraphic zones identified based on pollen and/or *sed*aDNA based CONISS zonations are indicated with Roman numerals. The *yellow band* marks the span of the proxy anomalies associated with the 8.2k climate event and *cyan bands* tree-cover decrease events occurring at 10.4 and 10.1 ka. Terrestrial pollen, NPP's, and charcoal are expressed as percentages vs. the terrestrial pollen sum, while for aquatic pollen the sum of terrestrial and aquatic pollen is used. Stomata are shown as absolute counts while for plant macrofossils the plus signs indicate an unquantified presence of finds. The *sed*aDNA data are expressed as number of occurrences in the eight PCR replicates. (For interpretation of the references to colour in this figure legend, the reader is referred to the web version of this article.)

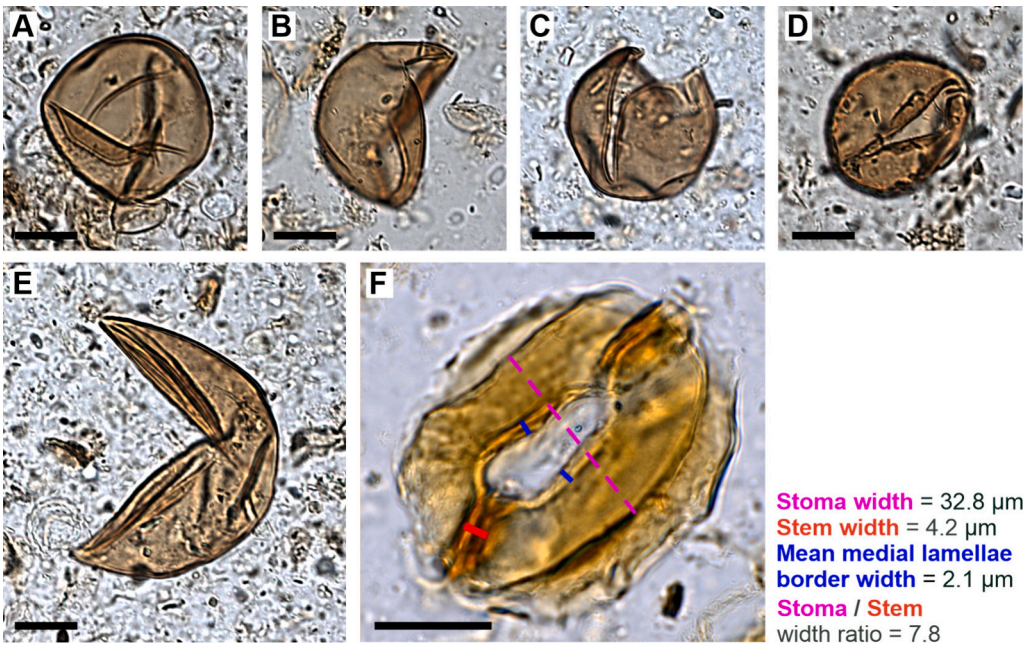

Fig. 6. Micrographs of (A–E) *Larix* pollen grains dating to 7.3–8.7 ka and (F) a *Picea* stoma dating to 8.7–8.9 ka from the Kuutsjärvi sequence. Diagnostic measurements for the *Picea* stoma are shown according to Sweeney (2004). Scale bars = 20 µm.

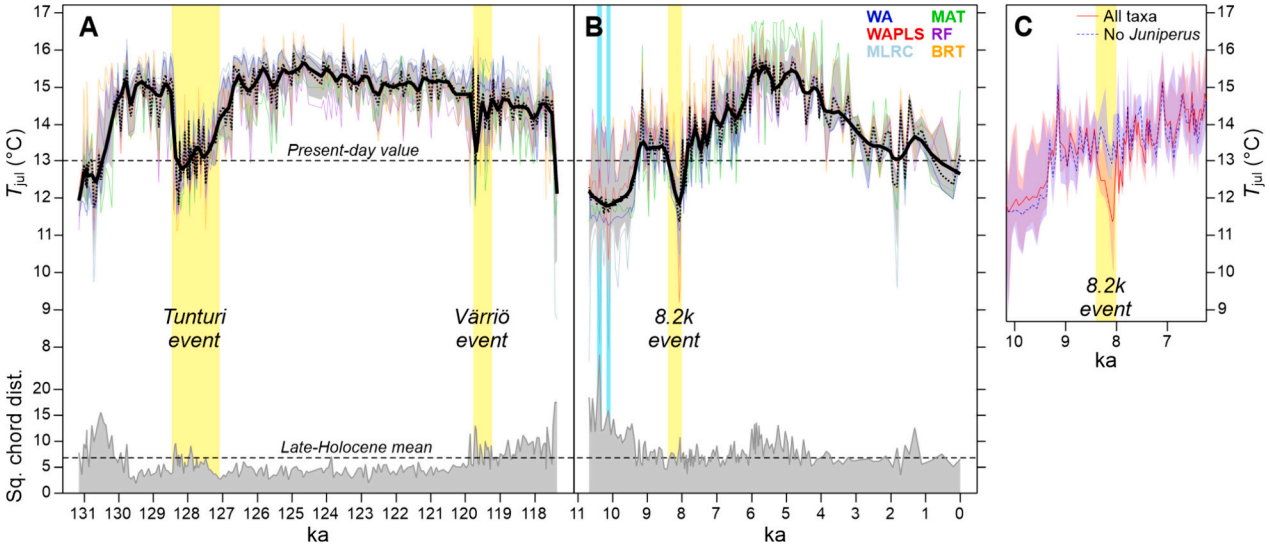

Fig. 7. Paleoclimate reconstructions from (A) the Last Interglacial sequence from Sokli (Salonen et al., 2018) and (B) the Holocene sequence from Kuutsjärvi. A six-method ensemble is used, including modern-analogue technique (MAT), weighted averaging (WA), weighted averaging-partial least squares (WAPLS), maximum likelihood response curves (MLRC), random forest (RF), and boosted regression tree (BRT), with *coloured lines* indicating individual models. The *black dotted line* indicates the multi-model median and the *thick black line* a LOWESS smoother fitted to the median (span 0.03 for LIG and 0.05 for Holocene, with one robustifying iteration added). The *grey band* indicates the 95% confidence interval of the median curve, estimated by calculating the median 1000 times using bootstrap samples of the individual reconstructions. *Grey silhouette curves* show the modern analogue quality, as the squared-chord distance (Overpeck et al., 1985) to the best fitting modern assemblage in the calibration dataset. The mean distance found for late-Holocene (4–0 ka) samples is shown for reference. Abrupt climate events are highlighted with *yellow bands* and other periods with vegetation or climatic dynamics discussed in the text with *cyan bands*. In (C), reconstructions spanning the 8.2k event (ensemble median and 95% confidence intervals) are shown for all pollen taxa but either including or excluding *Juniperus*. For the full ensemble reconstruction without *Juniperus*, see Fig. S7. (For interpretation of the references to colour in this figure legend, the reader is referred to the web version of this article.)

Holocene Thermal Maximum (HTM) at ca. 6–4 ka. During the HTM, reconstructed temperature remains around 2–2.5 °C above present, reaching the same level as reconstructed during the warm stages of the LIG (Fig. 7A). In the uppermost samples, the reconstruction converges well with the observed modern temperature, suggesting absence of persistent bias in the reconstruction.

For comparison with the pollen-based T_{jul}, Fig. 8A plots the proportion of *sed*aDNA reads for plants in the temperature optima classes of Tyler et al. (2021). Here, the main shift occurs over ca. 8–7 ka with both temperate taxa and arctic-alpine taxa being common in the early Holocene, while the past 7 ka are characterised by a more abundant occurrence of taxa from the middle of the temperature optimum scale.

Moisture requirement from *sed*aDNA (Fig. 8B) and pollen (Fig. 8C)

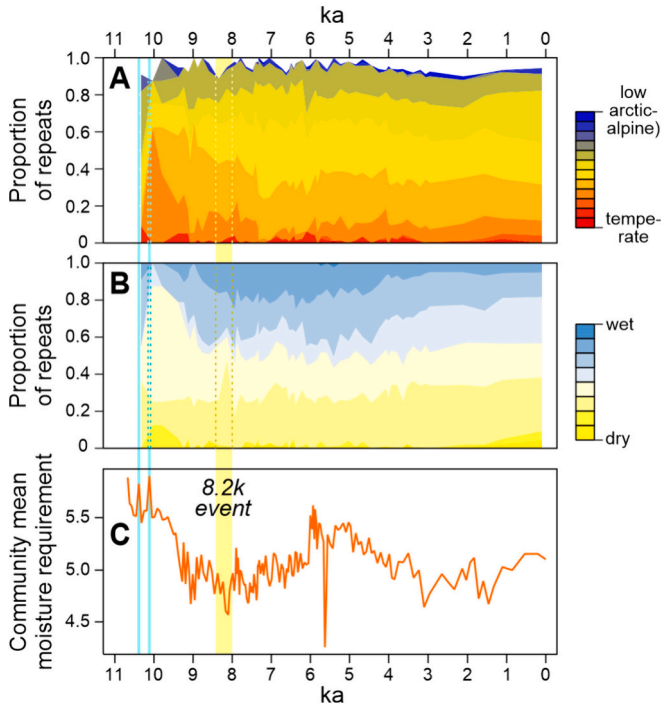

Fig. 8. Pollen and *sed*aDNA-based plant reconstructions for ecological indicator values, including the distribution of taxon-specific temperature optimum values (A) and moisture requirement values (B) for the *sed*aDNA PCR repeats, and (C) community-weighted moisture requirement of the vegetation around Kuutsjärvi calculated from the pollen data. The timing of the 8.2k climate event is highlighted with a *yellow band* and other periods with vegetation or climatic dynamics discussed in the text with *cyan bands*. (For interpretation of the references to colour in this figure legend, the reader is referred to the web version of this article.)

share the main feature of indicating moisture-demanding vegetation during the temperature maximum (Fig. 7B), with higher weighted average moisture requirement calculated from pollen and with taxa with high moisture requirement ($\geq$ 7) reaching peak values of 40% in the proportion of *sed*aDNA repeats over 6–4 ka, followed by a trend towards smaller moisture requirement during the past 4 ka. In addition, pollen shows a sharp dry spike at 5.6 ka, likely driven by an anomalous peak where *Pinus* pollen reaches a value of 87% (Fig. 5A), leading to a community-level moisture requirement minimum due to the low moisture requirement (4) of the sole Fennoscandian pine species *Pinus sylvestris*. Especially before 9 ka there is disagreement between the moisture requirements suggested by pollen and *sed*aDNA, indicating relatively wet vs. dry conditions, respectively. However, during the 8.2 ka cooling event, both pollen and *sed*aDNA show a sharp deviation towards low moisture requirements.

3.5. Climate simulations

In the CESM1 simulations (Fig. 9) the very early Holocene at 11 ka is still dominated by the presence of the retreating Fennoscandian Ice Sheet, and approximates the situation at the time of the deglaciation of Kuutsjärvi shortly afterwards. At around 11 ka, simulated July temperatures in northeastern and southern Finland were still 3 to 5 °C colder depending on the distance to the ice edge, with dominating westerly to northerly winds from the ice sheet and the cold Nordic Seas (Fig. 9A). These conditions rapidly improved with the ice retreat and continued high orbital summer insolation. By 9 ka, simulated July temperatures in south and central Finland started to exceed slightly pre-industrial (PI) levels by <1 °C around 9 ka, with values close to PI levels around Kuutsjärvi. In northern Finland, winds were now coming from the north counteracting the warming that was progressing in inland areas (Fig. 9C). Winter temperatures at 11 ka were very severe with mean January temperatures up to 40 °C colder than PI close to the ice sheet with westerly winds coming off the ice sheet (Fig. 9B). At 9 ka, winters were still ~30 °C colder in northern Finland with winds now coming from the south (Fig. 9D).

4. Discussion

The Kuutsjärvi sequence provides an interesting high-resolution proxy record of the early and mid Holocene, including the first Holocene record of larch presence in northern Finland, as well as a distinctive series of abrupt vegetation shifts with possible linkages to hemispheric climate events. We discuss these findings in the following sections, with main focus on early and mid Holocene compared to the late Holocene, where the Kuutsjärvi proxy resolution is limited due to the conspicuous shift to lower sedimentation rate at ~3.8 ka.

4.1. Holocene history of Larix and Picea

A noteworthy feature in the Kuutsjärvi fossil sequence are the *Larix* pollen grains (Fig. 6A–E) occurring in several samples dating to 9.6–5.9 ka (Fig. 5A), suggesting that Siberian larch (*Larix sibirica*) has grown in the area during the early Holocene. This is the first record demonstrating the early-Holocene presence of this tree species in northern Finland. Previously, it has been demonstrated that Siberian larch has occurred at its current western range margin in NW Russia from the early Holocene, with speculated presence also in southern Finland and Sweden (Kuosmanen et al., 2014; Kuosmanen et al., 2016). The larch pollen grain is heavy and known to have a limited dispersal distance (Burczyk et al., 2019) and therefore even rare occurrences can be considered as an indication of local presence (Jankovská et al., 2006). Even in situations where larch is the dominant tree species present, *Larix* pollen values can be as low as 0.5% (Kultti et al., 2003). *Larix* stomata are often found together with *Larix* pollen and considered as firm evidence of the presence of the species (Ammann et al., 2014). However, as with plant macrofossils in general, the occurrence of stomata is dependent on the taphonomic (accumulation and preservation) and the depositional environment (Leitner and Gajewski, 2004). Here, the lack of *Larix* macrofossils and stomata is concordant with the general lack of any macrofossils in the Kuutsjärvi record over the timeframe of the *Larix* pollen finds (Fig. S5), and may not be a reliable indication of a low population density of larch. More noteworthy is the lack of *Larix* *sed*aDNA, given the demonstrated ability of *sed*aDNA to pick up *Larix* even when the pollen grains are absent (Sjögren et al., 2017). Furthermore, conditions for DNA preservation cannot explain the lack of *Larix* *sed*aDNA. Although DNA fragmentation can result in molecules becoming too short for PCR metabarcoding, and therefore appearing to not be preserved, the targeted *Larix* barcode of 46 base pairs (bp) is either shorter than, or comparable to, barcodes for many of the other tree taxa that are well-detected in the Kuutsjärvi record (e.g. *Alnus*, 61 bp; *Betula*, 61 bp; *Salix*, 56 bp; *Pinus*, 45 bp). This precludes DNA preservation being the cause of *Larix* absence in our *sed*aDNA dataset. Hence, while even abundant presence of larch could not be ruled out based on the pollen levels observed at Kuutsjärvi, the lack of *sed*aDNA suggests larch was either relatively rare in the catchment or growing at some distance from the lake.

The lack of previous evidence for larch in Holocene records from Finland may be due to the notorious scarcity of *Larix* in pollen records. Moreover, the identification of its relatively nondescript (apart from large size) pollen grains (Fig. 6A–E) may have been omitted in earlier studies by analysts unfamiliar with the type. The occurrence of larch in the early Holocene in the Swedish Scandes was suggested by Kullman (1998) and Öberg and Kullman (2011) and there are records of Siberian larch growing in northern Finland during the Marine Isotope Stage 5e, 5c and 5a warm intervals (130–70 ka; e.g., Aalto et al., 1992; Forsström,

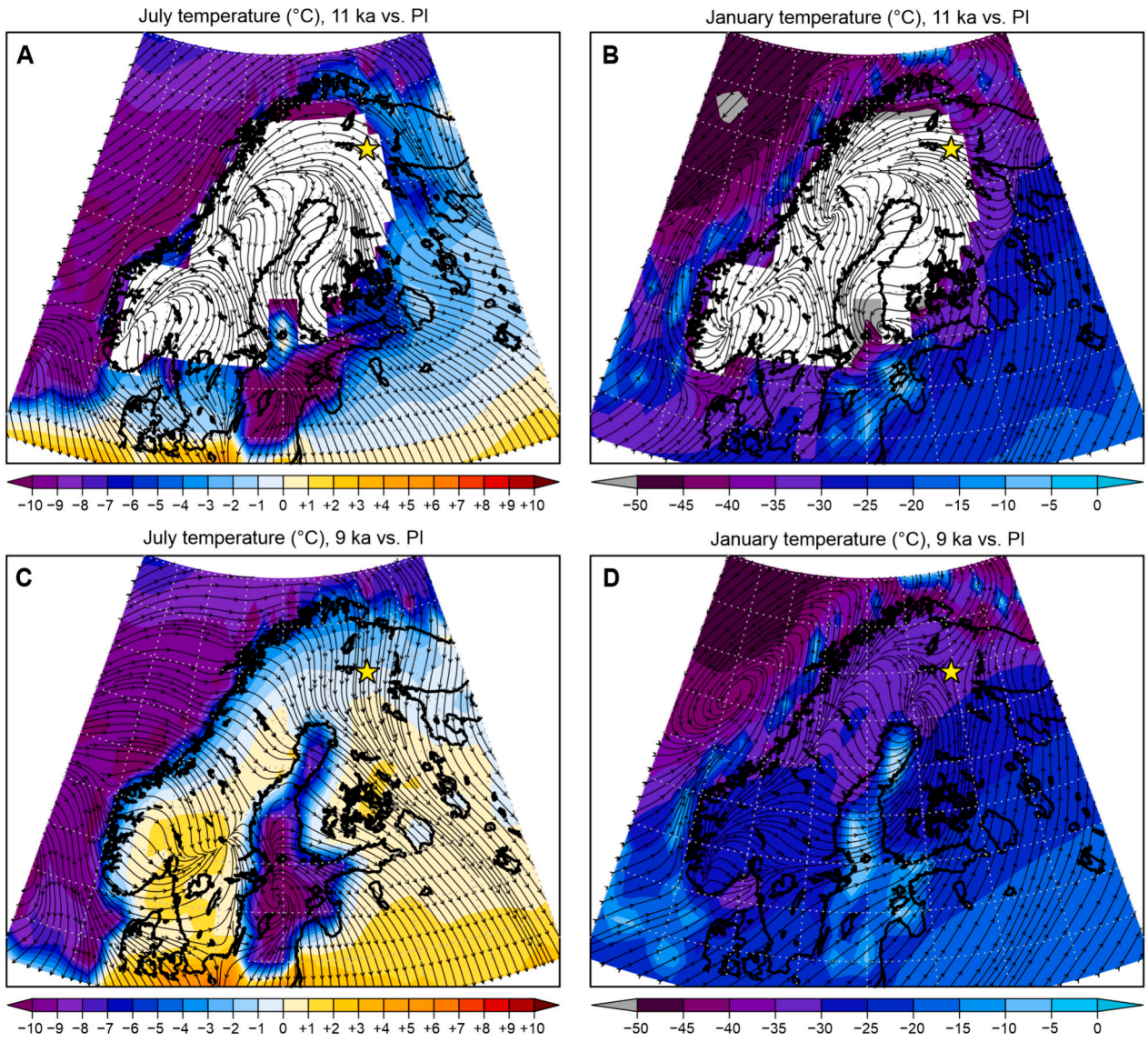

Fig. 9. Fennoscandian surface temperature anomalies relative to the pre-industrial as simulated by CESM1. The panels show July and January temperature anomalies vs. pre-industrial for 11 ka (A and B, respectively) and 9 ka (C and D). The *black streamlines with arrows* in each panel indicate the respective mean July or January near-surface wind field that dominated in past climate states and the *white area* gives the extent of the Fennoscandian ice sheet at 11 ka which melted away before 9 ka. A *yellow star* marks the location of Kuutsjärvi. (For interpretation of the references to colour in this figure legend, the reader is referred to the web version of this article.)

1990; Helmens et al., 2012; Helmens et al., 2021; Salonen et al., 2018). Furthermore, the fact that Siberian larch has been present at its western margin in NW Russia from the early Holocene (e.g., Clarke et al., 2020; Demidov and Lavrova, 2001; Filimonova, 2006; Kuosmanen et al., 2014; Kuosmanen et al., 2016) makes it plausible the species would have migrated further west in the suitable early-Holocene climate and open habitats.

The early Holocene at Kuutsjärvi also shows the presence of Norway spruce (*Picea abies*), indicated by pollen and stomata records and traces of spruce *sed*aDNA (Fig. 5A). It could be argued that the *Picea* pollen has been transported by wind, but the presence of a *Picea* stoma dated to 8.9–8.6 ka (Fig. 6F) provides clear evidence of the local presence of spruce trees (Clayden et al., 1996). Also, the spruce *sed*aDNA is found in three of five samples from 9.2 to 8.9 ka (Fig. 5A), which is higher than what has been recorded as background contamination for this species, based both on a previous study (1.99%, SD = 2.52, range 0–6.25 of 1360 the negative control PCR repeats of 170 negative control samples; Alsos et al., 2020) and the negative controls used here (1/104 PCR repeats from 13 negative controls). The presence of spruce is concordant with several studies suggesting that spruce was present in northern Finland during the late-glacial to early Holocene (e.g., Aario, 1943; Kanerva, 1956; Vasari, 1962). Spruce has most probably been growing in small populations as part of a mixed pine-birch forest. The disappearance of spruce pollen coincides with the 8.2 ka cold event and the evidence of increasing abundance of Siberian larch. It is plausible that drier and cooler conditions indicated by the paleoclimate reconstruction may have favoured Siberian larch as it endures more harsh winter conditions as their dense and falling needles may protect them from winter desiccation and wind abrasion (Gower and Richards, 1990). The Kuutsjärvi pollen record suggests that the larch population was most abundant at 8.7–7.3 ka, coinciding with a broad minimum in total tree pollen during and around the 8.2 ka event. As larch trees benefit from open and light-abundant growing conditions, this suggests an improved habitat for larch as a mixed species in the light pine-birch dominated forest around the lake. As the Holocene got warmer (Fig. 7B) and the forest cover denser, the growing conditions for larch deteriorated and the larch may

have been outcompeted by other species (Kharuk et al., 2007; Shuman et al., 2011). The clear increase in *Alnus* (alder) pollen at 6 ka suggests the development of a denser shrub layer, possibly increasing shading and hence creating unfavourable conditions for the regeneration of larch (Kharuk et al., 2007) which then disappears from the pollen record at 5.9 ka (Fig. 5A).

The expansion of the spruce population occurs in the late Holocene, whereas larch remains absent. In the early Holocene, both spruce and larch populations were most probably scattered and small satellite populations rather than the population front which likely remained further east or south-east at that time. It is likely that Siberian larch went regionally extinct in our study area due to less suitable growing conditions in the middle Holocene and remained near its current westernmost natural limit in NW Russia as shown by Kuosmanen et al. (2016). However, spruce may have remained as a scarce, mixed component of the northern boreal forests. In general, the expansion of spruce westward from NW Russia started in the middle Holocene and spruce took over the possible habitats (e.g., Kuosmanen et al., 2016; Seppä et al., 2009a). In NE Lapland, the spruce population expanded at around 2 ka, indicating a change to a more closed mixed coniferous forest. As spruce is a highly competitive species, it is plausible that having started its westward migration as the climate cooled, spruce outcompeted and prevented the westward migration of Siberian larch.

4.2. Early-Holocene climate shifts

4.2.1. Climate following deglaciation (10.7–9 ka)

In the Kuutsjärvi climate reconstruction (Fig. 7B) the largest spread between the individual calibration methods is seen for the tree *Betula*-dominated Zone I (10.7–9.3 ka). The classical methods (WA, WA-PLS, MLRC, MAT) show colder than present T_{jul} through Zone I, followed by a warming of ca. 2–3 °C at the transition to the *Pinus*-dominated Zone II at 9.2 ka. In comparison, the new machine-learning algorithms (BRT, RF) show Zone I temperatures at or slightly above present and no significant change moving to Zone II, after which the entire ensemble shows better convergence through the middle and late Holocene. Our climate model runs would support the significant warming at Kuutsjärvi over the early Holocene, with T_{jul} at 11 ka being up to 5–6 °C below the pre-industrial, in a region stretching several hundred kilometres from the eastern margin of the Fennoscandian ice sheet (Fig. 9A), but rising to <1 °C below pre-industrial conditions by 9 ka (Fig. 9C). Around 11 ka, Kuutsjärvi is close to the ice sheet edge, and in the model receives westerly winds (perhaps dry and katabatic) descending from the ice sheet (Fig. 9A). At 9 ka, the ice sheet is gone and weak northerly winds come from the north in summer and stronger winds from the south in winter (Fig. 9C). The cold coasts vs. warm interior continental pattern at 9 ka implies a dominance of autochthonous warming by high orbital insolation while winds from the sea would lead to cooling. These results are paralleled in the CHELSA-Trace21k transient modelling (Karger et al., 2023), showing T_{jul} in northeast Fennoscandia several degrees below present at the ice sheet margin at interglacial onset, but reaching approximately modern values by 10 ka as the ice sheet receded (Alsos et al., 2022).

However, the cooler than present temperatures at the onset of the Holocene are hard to reconcile with the multiproxy data from Lake Loitsana, located in the Sokli basin ca. 15 km NW of Kuutsjärvi. At Loitsana, plant macrofossil evidence for local occurrence of summer-temperature sensitive aquatic plants suggests temperatures at 10.5 ka already exceeded the present day by up to 2 °C. This is supported by chironomid-based T_{jul} reconstructions, which also indicate above-present values through the early Holocene (Shala et al., 2017), lending support to the warmest members of our reconstruction ensemble at 10.6–9.3 ka. Also at Kuutsjärvi, the early-Holocene *sed*aDNA record detects diverse plant assemblages, such as *Cicuta virosa*, *Sparganium*, *Potamogeton*, *Urtica dioica* and ferns, such as *Matteuccia struthiopteris* and *Thelypteris palustris* (Fig. 5B), suggesting warm T_{jul} of at least ~13 °C, inferred from their current distributions (Lampinen and Lahti, 2023; Väliranta et al., 2015; Venäläinen et al., 2005), and with the temperate taxa present from the base of the *sed*aDNA sequence at 10.5 ka (Fig. 10C). Similarly, both terrestrial and aquatic warm indicator taxa were found in *sed*aDNA studies north and west of Kuutsjärvi (Alsos et al., 2022; Revéret et al., 2023). Due to the presence of warmth indicators at a number of sites, we favour the interpretation that the conditions were regionally warm soon after deglaciation, at least during summers though not necessarily in winters, as discussed in the next subsection.

4.2.2. 10.3k event

The 10.4 and 10.1 ka tree pollen minima (Fig. 10G) are roughly contemporaneous with the 10.3k climate event widely described in Northern Hemisphere proxy data (e.g., Björck et al., 2001; Li et al., 2022). The 10.3k event coincides with one of the major glacial meltwater rerouting events which occurred in North America during the last deglaciation (R2; blue arrow in Fig. 10), starting a routing through the St. Lawrence River, lasting until the 8.2k event and its associated rerouting through the Hudson Bay (R1; Fig. 10) (Clark et al., 2001). The R2 rerouting at 10.3 ka aligns with the strongest Holocene excursion in North Atlantic benthic foraminifera $\delta^{13}C$ data, indicating a disturbance in Atlantic thermohaline circulation (Bond et al., 1997). More proximal to Kuutsjärvi, the event has been recorded as a fall in a pollen-based T_{jul} reconstruction in northern Norway (Seppä et al., 2002), a reduction in vegetation cover in northwest Russia (Karelian isthmus; Subetto et al., 2002), and a gap in the eastern Fennoscandian archaeological radiocarbon record, which may represent a severe decline in the local Mesolithic human population (Tallavaara et al., 2014). In these studies, the anomalies detected at 10.3 ka are described as a single event, while the Kuutsjärvi tree curve shows two distinct events separated by a full intervening recovery (Fig. 10G). However, Greenland ice-core $\delta^{18}O$ records also show a clear two-pronged structure to the negative anomalies (Fig. 10A; Rasmussen et al., 2007), as does a north China speleothem record indicating twin minima of East Asia summer monsoon over 10.51–10.25 ka (Li et al., 2022). The two Greenland $\delta^{18}O$ minima align with Kuutsjärvi 10.4 and 10.1 ka events when accounting for the 95% error margins of the Kuutsjärvi age–depth model (ca. 370 years at 10.4–10.1 ka; error bar in Fig. 10) and the counting error of the GICC05 ice-core chronology (89 years at 10.3 ka; Rasmussen et al., 2007), allowing a hemispheric climatic linkage for the Kuutsjärvi events.

In the pollen-based T_{jul} reconstruction, the 10.4 and 10.1 ka tree minima are not robustly reconstructed as coolings (Fig. 10B), with the MLRC calibration model indicating a T_{jul} fall of ca. 3 °C at both 10.4 and 10.1 ka events and WA-PLS a 1–2 °C fall at 10.1 ka only, while the T_{jul} shifts are not beyond the range of centennial background variation in the remaining calibration models (Fig. 7B). However, the ability of the calibration models to reconstruct temperature fluctuations during this interval may be inhibited by the poor quality of modern pollen analogues during Zone I (10.6–9.3 ka) (Fig. 7B). In particular, the *Betula* percentages of ca. 80% and reaching up to 90% are beyond the variation seen in the calibration data, where only 2% of samples record *Betula* at over 60% and the maximum reached is 74%. It is doubtful that the pollen–climate calibration models could reliably infer climate shifts for the 10.4 and 10.1 ka events when the main pollen signal is a drastic *Betula* fall (Fig. 5A) from a high baseline level not covered by the calibration data.

We regard it likely that the 10.4 ka and 10.1 ka events at Kuutsjärvi are climatically driven, because given that the proxies for deep ocean ventilation indicate a disturbance in AMOC during the 10.3k event (Bond et al., 1997), a climatic impact extending to northern Fennoscandia would be expected. While the cooling would explain the loss in tree cover (Fig. 10G), the drought also predicted by proxy evidence and climate model simulations for AMOC-driven abrupt events (Alley and Ágústsdóttir, 2005; Drobyshev et al., 2016; Renssen et al., 2018) would explain the charcoal peaks (Fig. 10F) through increased wildfires. The opening of the vegetation would, in turn, result in an increased presence

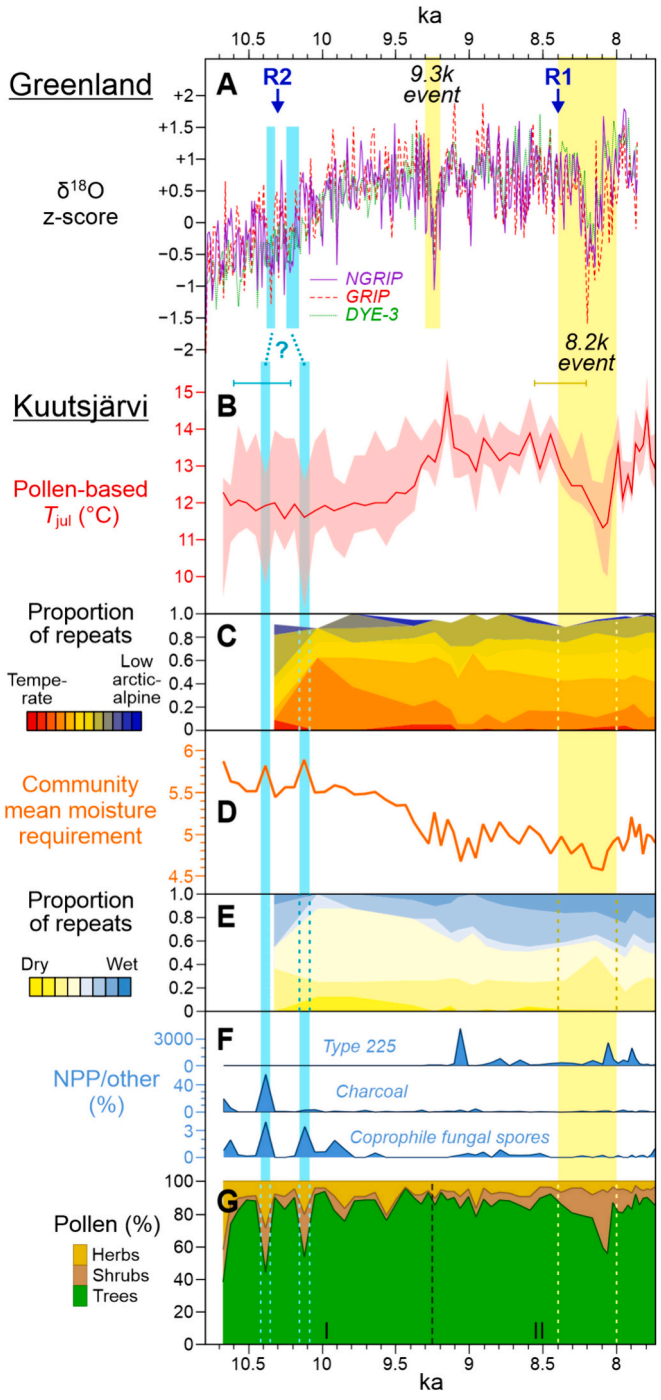

(caption on next column)

Fig. 10. Comparison of early-Holocene data from Greenland (A) and Kuutsjärvi (B–G): (A) oxygen isotope data from three Greenland ice cores expressed as z-scores calculated from 10-year averages (Rasmussen et al., 2007); (B) pollen-derived July mean temperature (T_{jul}) reconstruction with the ensemble median (*solid line*) and its 95% error margins (*shading*); (C) distribution of taxon-specific temperature optimum values (Tyler et al., 2021) for the *sed*aDNA PCR repeats; (D) community-weighted moisture requirement of the vegetation around Kuutsjärvi calculated from the pollen data; (E) distribution of taxon-specific moisture requirement values (Tyler et al., 2021) for the *sed*aDNA PCR repeats; (F) selected non-pollen palynomorphs (NPP's) and charcoal; (G) pollen data divided in herb, shrub, and tree components, with biostratigraphic zones marked with Roman numerals. The *yellow bands* show the spans of Greenland ice-core proxy anomalies for the 8.2k (8.4–8.0 ka; Alley et al., 1997) and 9.3k (approximately 9.3–9.2 ka; Rasmussen et al., 2007) climate events. The *cyan bands* show the 10.4 and 10.1 ka tree-cover decrease events in the Kuutsjärvi data, and the possibly correlated cold intervals associated with the 10.3 ka cold event in the Greenland data. The *error bars* in panel B show the 95% age range of the Kuutsjärvi age–depth model at the 10.4 ka event and the onset of the 8.2k event. The *blue arrows* in panel A show the timing of the North American freshwater rerouting events R2 (10.3 ka) and R1 (8.4 ka) (Clark et al., 2001). (For interpretation of the references to colour in this figure legend, the reader is referred to the web version of this article.)

of reindeer (*Rangifer tarandus*), reflected in the peaks of coprophile fungal spores (Fig. 10F). However, as the age-depth model of Kuutsjärvi and its uncertainties allow, but cannot prove, the contemporaneity of the 10.4 ka and 10.1 ka tree-pollen minima with the circum-North Atlantic 10.3k event, an alternative explanation is that a local disturbance by herbivory was the proximal cause for the tree-cover decrease. Here, herbivory by reindeer is the more feasible explanation, as herbivory by insect larvae commonly affecting modern-day Finnish Lapland mountain birch (*Betula pubescens* subsp. *tortuosa*) – the presumed sole tree species around Kuutsjärvi during the 10.4 and 10.1 ka tree-cover decrease events – should have been constrained by cold early-Holocene winters.

The climate simulations for 11 ka (Fig. 9B) and 9 ka (Fig. 9D) suggest mean January temperatures being >30 °C below pre-industrial levels (~ −13 °C) at Kuutsjärvi. These severe modelled winter temperatures cannot conclusively be validated against data, due to the lack of robust winter paleotemperature proxies in the European Arctic. However, the temperature optimum distribution in the *sed*aDNA data at 10.3 ka (Fig. 10C), with co-occurring temperate and arctic-alpine species, hints to a high-continentality regime and thus cold winters. Winters to any degree colder than present would make herbivory by insects unlikely, as the maximal cold tolerances for *Epirrita autumnata* (Virtanen et al., 1998) and *Operophtera brumata* (Ammunét et al., 2012) moth eggs are estimated at −35.5 °C and − 35 °C, respectively, and these limits have been exceeded at the Värriötunturi meteorological station adjacent to Kuutsjärvi already in the 1991–2020 observational period (−38.3 °C in 1999; Jokinen et al., 2021). By contrast, the climate modelling suggests that winter temperatures may have been close to the survival threshold of mountain birch, with a cold tolerance estimated at −36 °C. Hence, any further cooling spikes beyond the cold early-Holocene baseline could explain the tree-cover decrease events consisting of sharp minima in tree-type *Betula* pollen. An additional possibility is that herbivory by increased reindeer populations functioned as a positive feedback to a climatically initiated tree-cover loss.

4.2.3. 8.2k event

In contrast to the 10.4 and 10.1 ka pollen anomalies, the tree pollen minimum at 8.38–8.02 ka (Fig. 10G) is reconstructed as a sharp T_{jul} fall by all members of the calibration model ensemble (Fig. 10B). This T_{jul} anomaly falls neatly within the 8.4–8.0 ka time window associated with the 8.2k climate event in Greenland ice cores (Fig. 10A) (Alley et al., 1997). Based on the timing and shared temporal structure, including a gradual decline but a sharper recovery seen in both Greenland ice cores (Fig. 10A) and at Kuutsjärvi (Fig. 10G), we suggest the Kuutsjärvi forest

decline event represents a northern Fennoscandian signal of this global event driven by a disruption of the Atlantic Meridional Overturning Circulation (AMOC) (Alley and Ágústsdóttir, 2005). While the proxy anomalies of the 8.2k event are generally strongest downwind of the North Atlantic (Alley and Ágústsdóttir, 2005), earlier work in Fennoscandia has failed to identify a signal of the event in the northern subarctic region (Seppä et al., 2007). By contrast, a clear signal is seen in pollen data and pollen-based temperature reconstructions from southern Finland (Heikkilä and Seppä, 2003; Sarmaja-Korjonen and Seppä, 2007) and Estonia (Veski et al., 2004), ca. 600–1000 km south of Kuutsjärvi.

In the Kuutsjärvi pollen data, the 8.2k event largely consists of a strong *Juniperus* maximum, resulting in corresponding minima in the total tree curve and its most abundant constituents *Alnus, Betula*, and *Pinus* (Fig. 5A). This strong signal of *Juniperus* is echoed and replicated in the *sed*aDNA data at 8.1 ka, whereas *Juniperus* is undetected at 8.4 and 7.9 ka. In the modern pollen data used for the pollen–T_{jul} calibration models, *Juniperus* shows a strong maximum in mountainous parts of western Scandinavia where it reaches values of 15–25% while largely remaining below 4% in the rest of the calibration data (Fig. S7). As a result, *Juniperus* is a strong indicator of cool summers in the calibration models, with a unimodal T_{jul} optimum of 12.6 °C in the WA model, well below the optima of the dominant trees in the Kuutsjärvi data, *Alnus* (15.7 °C), *Betula* (13.9 °C), and *Pinus* (14.6 °C). In the machine-learning based BRT and RF models, *Juniperus* is also heavily employed, being the third and fourth most important T_{jul} predictor in these models respectively, while the partial-dependency plots of the BRT model (Salonen et al., 2018) show that *Juniperus* is specifically a cold indicator, with values above 10% associated with T_{jul} below 14 °C. A reconstruction of the 8.2k event with *Juniperus* excluded from the pollen data (Fig. 7C) shows that, without *Juniperus*, the reconstructed T_{jul} variations during the 8.2k event no longer stand out from the baseline sample-to-sample noise.

Hence, while the Kuutsjärvi pollen record suggests that the 8.2k event had a major impact on the vegetation in northeast Finland, the interpretation that this represents, in particular, a fall in summer temperature hinges on *Juniperus* pollen, and thus the ecology of the underlying species, *Juniperus communis*, merits further discussion. Notably, a similar strong response of *Juniperus* is repeated during the abrupt Tunturi event recorded in the LIG sequence of nearby Sokli (Fig. 7A), also linked to an AMOC disruption (Salonen et al., 2018), although the Tunturi event also shows a major shift in the *Betula/Pinus* ratio and an increase in herbs (Salonen et al., 2018) not seen during the 8.2k event at Kuutsjärvi.

In the ecological literature, *J. communis* is described as frost-tolerant, highly tolerant of poor soils, light demanding and intolerant of heavy shade, and tolerant of all but the severest drought (Thomas et al., 2007). Considering the ecology of *J. communis*, compared to the other species showing major responses at Kuutsjärvi during the 8.2k event, we suggest that the pattern of vegetation impact through northern Europe is best explained as a response to the drought combined with winter-dominant cooling. These, based on proxy data synthesis and climate simulations, have been suggested as relevant climatic signals in Europe in response to abrupt events driven by AMOC disruptions, including both the 8.2k (Alley and Ágústsdóttir, 2005) and Younger Dryas events (Denton et al., 2005; Schenk et al., 2018), in addition to other climate anomalies characterised by increased fire activity in northern Scandinavia during North Atlantic cooling events of the Holocene (Drobyshev et al., 2016). First, a strong summer temperature cooling appears unfeasible as a signal of the 8.2k event due to the lack of record of the event in pollen-based T_{jul} reconstructions from northern Fennoscandia (Seppä et al., 2007), despite summer temperature being the dominant ecological control on vegetation in this region (Blok et al., 2011; Elmendorf et al., 2012). Second, a winter-dominant cooling, as suggested by Seppä et al. (2007), could explain the pattern where the event is robustly reconstructed from pollen further south, in southern Fennoscandia and the Baltic states. Here the temperate broadleaf vegetation would be sensitive to cold in early spring and the onset of the growing season, while in northern Fennoscandia the subarctic vegetation would still be dormant and thus unaffected. However, despite the lack of signal in earlier pollen-based T_{jul} reconstructions, a similar rise in *Juniperus* pollen, as seen at Kuutsjärvi, has been broadly recorded in other pollen sequences from northern Fennoscandia at ca. 8.5–7.0 ka (Mäkelä et al., 1994; Seppä et al., 2002), with linkages proposed both to the 8.2k event (Seppä et al., 2002) and to the general vegetation succession and its impact on light availability for juniper (Mäkelä et al., 1994).

Finally, in addition to cooling, the strong vegetation disruption seen around Kuutsjärvi could also, in some part, be linked to the drought predicted by model simulations for an AMOC-driven climate event. At Kuutsjärvi, a possible indication of drought during the 8.2k event is seen in the sharp maximum of Type-225 NPP (Fig. 10F), a suspected algal spore (Van Geel et al., 1989) associated with dynamic water conditions, e.g. shallow or fluctuating water levels, as well as eutrophic to mesotrophic open water (Kuhry, 1997). During the Tunturi cooling event recorded at Sokli during the LIG (Fig. 7A), also suggested to be AMOC-driven, a mass occurrence of Type-225 co-occurs with a peak of *Spirogyra* green algae (Salonen et al., 2018) common in shallow, stagnant water (Van Der Wiel, 1982; Van Geel et al., 1983), supporting the association of Type-225 with low water levels. A moisture deficit could also explain the preferential survival of the drought-resistant juniper at the expense of other trees. Looking at moisture requirements of *J. communis* compared to major trees likely occurring around Kuutsjärvi at 8.5–8.0 ka, expressed as Ellenberg indicator values (Tyler et al., 2021) on a scale from 1 (very dry) to 8 (wet), *J. communis* has a moisture requirement of 4, which is lower or equal compared to *Alnus glutinosa* (8), *A. incana* (7), *Betula pendula* (4), *B. pubescens* (7), *Larix sibirica* (5), *Picea abies* (6), and *Pinus sylvestris* (4). Accordingly, the moisture requirement of the vegetation around Kuutsjärvi reaches an early-Holocene minimum at the peak of the 8.2k event (Fig. 10D,E). Regardless of the initial triggering climatic factor (cooling and/or drought), the opening of the canopy would further favour the light-demanding *J. communis*, and contribute to the strong *Juniperus* pollen and *sed*aDNA peaks (Fig. 5A), and tree pollen minimum (Fig. 10G), which developed at Kuutsjärvi synchronously with the Greenland isotopic event (Fig. 10A).

Overall, the difficulty of pinpointing the climate factor responsible for the 8.2k event vegetation response highlights the challenges potentially faced in climate reconstructions, especially when significant correlations between ecologically important variables exist in the region used in the modern-world proxy calibration (Chevalier et al., 2020; Juggins, 2013). While the *Juniperus* pollen maximum of the 8.2k event seen at Kuutsjärvi results in a reconstructed summer cooling, this is likely a spurious feature driven by the low summer temperatures in the modern-day Scandinavian mountains where the common occurrence of juniper (Fig. S7) may be proximally controlled by other factors. For example, competition from taller boreal plants with dense foliage can result in shading and reduce the amount of sunlight reaching juniper individuals, potentially affecting their seedling development and growth. Consequently, both the semi-open forest limit ecotone and open tundra, typically found in the mid-elevations of the Scandinavian mountains, are particularly favourable habitats for the species. In paleoenvironmental research, multiproxy studies as well as a thorough understanding of the underlying ecology can be important in detecting such proxy-specific biases.

4.3. Mid and late Holocene

In the Kuutsjärvi pollen-based climate reconstruction, the peak T_{jul} anomaly of 2–2.5 °C at 6–4 ka (Fig. 7B) is consistent with HTM anomalies seen for other northern high-latitude locations, generally falling between 1 and 3 °C (e.g., Kaufman et al., 2020b; Renssen et al., 2012; Sundqvist et al., 2010). It is also comparable with the T_{jul} reconstructed at Sokli for the warmest stages of the LIG (Fig. 7A). However, this

comparison only considers the summer season. For the Sokli LIG sequence, pollen-based January temperature reconstructions as well as supporting evidence from diatoms suggest mild winters coinciding with warmer than present summers, particularly in the late LIG (Plikk et al., 2016; Salonen et al., 2018; Salonen et al., 2021). Similar multiproxy constraints on the winter half-year conditions are not available for Kuutsjärvi, precluding the comparison of mean annual temperature anomalies for the HTM and the LIG.

The dominant feature of the Kuutsjärvi pollen sequence during the HTM is the strong maximum of alder (*Alnus*), rising to ~20% between 6.0 and 4.8 ka, at the same period when *Alnus* was also detected in all *sed*aDNA repeats, suggesting that it was growing close to the lake (Alsos et al., 2018). While both methods only identified *Alnus* at genus level, and the records could represent the currently common *A. incana*, we consider it possible that *A. glutinosa* was also growing around Kuutsjärvi during the HTM. In modern Fennoscandia, *A. glutinosa* has its present northern distribution limit in central Finland, several hundred km south of Kuutsjärvi, while *A. incana* is common throughout Fennoscandia, growing also in the open vegetation types of the northernmost regions. The vegetation assemblages after the rise of the *Alnus* curve at 9.2 ka clearly show that moist habitats were abundantly available around Kuutsjärvi for the more moisture-demanding (Tyler et al., 2021) *A. glutinosa*. The assemblage identified with *sed*aDNA (Fig. 5B) includes aquatic taxa (*Callitriche* and *Potamogeton*) and taxa that thrive on creek banks, wet depressions and limnotelmatic conditions (*Cicuta virosa*, *Caltha palustris*, *Hippuris*, *Filipendula ulmaria*, and ferns). Of ferns, *Phegopteris connectilis* and *Matteuccia struthiopteris* need shade and currently typically occur in lush (spruce) forest environments. The moist environmental conditions can at least partially be ascribed to the setting of Kuutsjärvi in a canyon-like depression with bedrock at or close to the surface. We note that in the nearby Loitsana lake (~10 km west of Kuutsjärvi), similar *Alnus* values of 20% are recorded, however considerably earlier (ca. 8–7 ka) compared to Kuutsjärvi (Salonen et al., 2013). The disparate timing of the strong *Alnus* pollen peaks at these nearby sites suggests that the mid-Holocene *Alnus* maxima are significantly modulated by local wetland habitat availability, in addition to the underlying climatic warming allowing the alder expansion. By extension, it is possible that the short reconstructed HTM at Kuutsjärvi at 6–4.8 ka (Fig. 7B) is a byproduct of these non-climatic controls on *Alnus* occurrence, and only captured a part of a longer HTM (ca. 8–4 ka) reconstructed in earlier northern-European multisite syntheses (Davis et al., 2003; Salonen et al., 2014; Seppä et al., 2009b).

The shift to a lower sedimentation rate at ~3.8 ka (Fig. 2) considerably hampers the late-Holocene proxy resolution at Kuutsjärvi. Multiple possible contributors to this shift can be identified. First, the Kuutsjärvi bathymetry (Fig. 1C) reveals several bowl-shaped hollows, including our coring site. Initially sedimentation was focused in these hollows, followed by the spread of sedimentation over a larger part of the lake basin, leading to reduced sedimentation rates. A further possible cause is a change in basin hydrology, suggested by the occurrence of the yellow algal bands in the stratigraphy (Fig. 5A). Relatively low lake levels in the early- and middle-Holocene possibly resulted in a closed basin where Kuutsjärvi had no or a limited outlet. Stratified conditions in the deep and sheltered lake (and further promoted by warm summers; Fig. 7B), with recycling of nutrients from bottom sediment, resulted in high nutrient levels and the temporal algal blooms indicated by the yellow bands. At the transition to the late Holocene, the algal bands disappear from the lithology, contributing to the reduction in sedimentation rate, possibly due to increased water flow through to the lake breaking up the stratification. The temporal spread in macrofossil dates at 69–73 cm depth (Fig. 2), contributing to the larger modelled age errors from ~3.8 ka onward, could also be explained by slumping of sediment along the sides of the basin due to the increased water flow. In addition, the reduced deposition of organic matter suggested by the decrease in loss-on-ignition (Fig. 5A), due to either organic matter washing out of the lake or reduced productivity in the cooler climate, further slowed down the sedimentation rate.

5. Conclusions

- We present a robustly dated core sequence from Lake Kuutsjärvi, NE Finland, providing high-resolution records of pollen, *sed*aDNA, plant macrofossils, conifer stomata and non-pollen palynomorphs for the past 10.6 ka.
- The Kuutsjärvi data indicate an early arrival of spruce by 9.2 ka (pollen, *sed*aDNA, and stoma finds), as well as the first evidence for the Holocene presence of larch in Finland, with pollen finds dating to 9.6–5.9 ka.
- Two strong tree pollen minima were detected at 10.4 and 10.1 ka, coinciding with spikes in charcoal and coprophile fungal spores. We interpret these tree-cover decrease events to represent a two-pronged signal of the 10.3k climate event, with cooling and drought resulting in forest loss, wildfires and increased reindeer populations.
- The Kuutsjärvi sequence shows a clear signal of the 8.2k event, previously poorly documented in northern Fennoscandia, with a collapse of the pine-birch forest and replacement by juniper developing in tight synchrony with Greenland isotopic proxies over 8.4–8.0 ka. We interpret this vegetation impact to result from some combination of drought and likely winter-dominant cooling, with the following opening of the forest vegetation contributing to the strong maximum of the cold- and drought-hardy but light-demanding juniper.

CRediT authorship contribution statement

J. Sakari Salonen: Writing – review & editing, Writing – original draft, Visualization, Validation, Project administration, Methodology, Investigation, Funding acquisition, Formal analysis, Data curation, Conceptualization. **Niina Kuosmanen:** Writing – review & editing, Writing – original draft, Investigation, Data curation. **Inger G. Alsos:** Writing – review & editing, Writing – original draft, Project administration, Methodology, Investigation, Funding acquisition, Formal analysis, Data curation. **Peter D. Heintzman:** Writing – review & editing, Writing – original draft, Visualization, Validation, Methodology, Funding acquisition, Formal analysis, Data curation. **Dilli P. Rijal:** Writing – review & editing, Writing – original draft, Visualization, Methodology, Investigation, Formal analysis, Data curation. **Frederik Schenk:** Writing – review & editing, Writing – original draft, Visualization, Methodology, Investigation, Formal analysis. **Freja Bogren:** Writing – original draft, Investigation, Formal analysis. **Miska Luoto:** Writing – review & editing, Writing – original draft, Investigation, Formal analysis, Data curation. **Annemarie Philip:** Writing – original draft, Investigation, Formal analysis. **Sanna Piilo:** Investigation, Formal analysis. **Liva Trasune:** Writing – original draft, Visualization, Investigation, Formal analysis. **Minna Väliranta:** Writing – review & editing, Writing – original draft, Methodology, Investigation, Formal analysis, Data curation. **Karin F. Helmens:** Writing – review & editing, Writing – original draft, Visualization, Validation, Project administration, Methodology, Investigation, Data curation, Conceptualization.

Declaration of competing interest

The authors declare the following financial interests/personal relationships which may be considered as potential competing interests:

Sakari Salonen reports financial support was provided by Academy of Finland. Frederik Schenk reports financial support was provided by Swedish Research Council Formas. Inger Alsos reports financial support was provided by European Research Council. Peter Heintzman reports financial support was provided by Knut and Alice Wallenberg Foundation. Dilli Rijal reports financial support was provided by Research Council of Norway. Peter Heintzman reports financial support was provided by Research Council of Norway.

Data availability

A supplementary data file is included in this submission. The file supplementary data is hosted externally on Figshare.

Salonen_ea-Kuutsjarvi-Supplementary_data.xlsx (Original data) (Figshare)

Acknowledgements

We thank Lilia Orozco and Maija Heikkilä for help with radiocarbon dating, Antti Ojala, Jan Weckström and the Värriö Research Station personnel for assistance during the fieldwork, Marco Milardi for the bathymetry data, Erik Schytt Mannerfelt for the drone imagery, and Dr. Helena Svitavská Svobodová for help with *Larix* pollen identification. JSS received funding from the Academy of Finland (projects 278692, 310649, and 331426), FS from the Swedish Research Council for Sustainable Development (FORMAS 2020-01000 and 2023-01631), IGA from European Research Council (ERC) under the European Union's Horizon 2020 research and innovation program grant agreement no. 819192, PDH from the Knut and Alice Wallenberg Foundation (KAW 2021.0048 and KAW 2022.0033), and PDH and DPR from the Research Council of Norway grant 250963/F20 for the ECOGEN project; the latter also supported the *sed*aDNA analyses. Bioinformatic processing was performed on resources provided by UNINETT Sigma2–the National Infrastructure for High Performance Computing and Data Storage in Norway (projects nn9848k and nn9854k). The climate model simulations with CESM1 were enabled by resources provided by the National Academic Infrastructure for Supercomputing in Sweden (NAISS) at Linköping University, partially funded by the Swedish Research Council through grant agreement no. 2022-06725.

Appendix A. Supplementary data

Supplementary data to this article can be found online at https://doi.org/10.1016/j.gloplacha.2024.104462.

References

Aalto, M., Eriksson, B., Hirvas, H., 1992. Naakenavaara Interglacial—a till-covered peat deposit in western Finnish Lapland. B. Geol. Soc. Finl. 64, 169–181. https://doi.org/10.17741/bgsf/64.2.005.

Aario, L., 1943. Über die Wald- und Klimaentwicklung an der Lappländischen Eismeerküste in Petsamo. Mit einem Beitrag zur Nord- und Mittel- Europäischen Klimageschichte. Ann. Bot. Soc. Zool. Bot. Fenn. Vanamo 19, 1–158 (In German).

Alley, R., Ágústsdóttir, A., 2005. The 8k event: cause and consequences of a major Holocene abrupt climate change. Quat. Sci. Rev. 24, 1123–1149. https://doi.org/10.1016/j.quascirev.2004.12.004.

Alley, R.B., Mayewski, P.A., Sowers, T., Stuiver, M., Taylor, K.C., Clark, P.U., 1997. Holocene climatic instability: a prominent, widespread event 8200 yr ago. Geology 25, 483–486. https://doi.org/10.1130/0091-7613(1997)025%3C0483:HCIAPW%3E2.3.CO;2.

Alsos, I.G., Lammers, Y., Yoccoz, N.G., Jørgensen, T., Sjögren, P., Gielly, L., Edwards, M. E., 2018. Plant DNA metabarcoding of lake sediments: how does it represent the contemporary vegetation. PLoS One 13, e0195403. https://doi.org/10.1371/journal.pone.0195403.

Alsos, I.G., Sjögren, P., Brown, A.G., Gielly, L., Merkel, M.K.F., Paus, A., Lammers, Y., Edwards, M.E., Alm, T., Leng, M., Goslar, T., Langdon, C.T., Bakke, J., van der Bilt, W.G.M., 2020. Last Glacial Maximum environmental conditions at Andøya, northern Norway; evidence for a northern ice-edge ecological "hotspot". Quat. Sci. Rev. 239, 106364 https://doi.org/10.1016/j.quascirev.2020.106364.

Alsos, I.G., Rijal, D.P., Ehrich, D., Karger, D.N., Yoccoz, N.G., Heintzman, P.D., Brown, A. G., Lammers, Y., Pellissier, L., Alm, T., Bråthen, K.A., Coissac, E., Merkel, M.K.F., Alberti, A., Denoeud, F., Bakke, J., 2022. Postglacial species arrival and diversity buildup of northern ecosystems took millennia. Sci. Adv. 8, eabo7434 https://doi.org/10.1126/sciadv.abo7434.

Ammann, B., van der Knaap, W.O., Lang, G., Gaillard, M.-J., Kaltenrieder, P., Rösch, M., Finsinger, W., Wright, H.E., Tinner, W., 2014. The potential of stomata analysis in conifers to estimate presence of conifer trees: examples from the Alps. Veg. Hist. Archaeobotany 23, 249–264. https://doi.org/10.1007/s00334-014-0431-9.

Ammunét, T., Kaukoranta, T., Saikkonen, K., Repo, T., Klemola, T., 2012. Invading and resident defoliators in a changing climate: cold tolerance and predictions concerning extreme winter cold as a range-limiting factor. Ecol. Entomol. 37, 212–220. https://doi.org/10.1111/j.1365-2311.2012.01358.x.

Birks, H.H., 2013. Plant Macrofossil Introduction. In: Elias, S.A., Mock, C.J. (Eds.), Encyclopedia of Quaternary Science, Second edition. Elsevier, Amsterdam, pp. 593–612.

Birks, H.J.B., Line, J.M., 1992. The use of Rarefaction Analysis for estimating Palynological Richness from Quaternary Pollen-Analytical Data. Holocene 2, 1–10. https://doi.org/10.1177/095968369200200101.

Birks, H.J.B., Braak, C.J.F.T., Line, J.M., Juggins, S., Stevenson, A.C., Battarbee, R.W., Mason, B.J., Renberg, I., Talling, J.F., 1990. Diatoms and pH reconstruction. Philos. Trans. R. Soc. B 327, 263–278. https://doi.org/10.1098/rstb.1990.0062.

Björck, S., Rundgren, M., Ingólfsson, Ó., Funder, S., 1997. The Preboreal oscillation around the Nordic Seas: terrestrial and lacustrine responses. J. Quat. Sci. 12, 455–465. https://doi.org/10.1002/(SICI)1099-1417(199711/12)12:6%3C455::AID-JQS316%3E3.0.CO;2-S.

Björck, S., Muscheler, R., Kromer, B., Andresen, C.S., Heinemeier, J., Johnsen, S.J., Conley, D., Koç, N., Spurk, M., Veski, S., 2001. High-resolution analyses of an early Holocene climate event may imply decreased solar forcing as an important climate trigger. Geology 29, 1107–1110. https://doi.org/10.1130/0091-7613(2001)029%3C1107:HRAOAE%3E2.0.CO;2.

Bjune, A.E., Greve Alsos, I., Brendryen, J., Edwards, M.E., Haflidason, H., Johansen, M.S., Mangerud, J., Paus, A., Regnéll, C., Svendsen, J.-I., Clarke, C.L., 2022. Rapid climate changes during the Lateglacial and the early Holocene as seen from plant community dynamics in the Polar Urals, Russia. J. Quat. Sci. 37, 805–817. https://doi.org/10.1002/jqs.3352.

Blaauw, M., Christen, J.A., 2011. Flexible paleoclimate age-depth models using an autoregressive gamma process. Bayesian Anal. 6, 457–474. https://doi.org/10.1214/11-BA618.

Blaauw, M., Christen, J., Aquino Lopez, M., 2022. rbacon: Age-Depth Modelling using Bayesian Statistics, R package version 2.5.8. https://CRAN.R-project.org/package=rbacon (accessed 30 April 2024).

Blok, D., Schaepman-Strub, G., Bartholomeus, H., Heijmans, M.M.P.D., Maximov, T.C., Berendse, F., 2011. The response of Arctic vegetation to the summer climate: relation between shrub cover, NDVI, surface albedo and temperature. Environ. Res. Lett. 6, 035502 https://doi.org/10.1088/1748-9326/6/3/035502.

Bogren, F., 2019. Evidence for Birch Forests and a Highly Productive Environment near the Margin of the Fennoscandian Ice Sheet in the Värriötunturit Area, Northeastern Finland.. M.Sc. thesis. Department of Physical Geography, Stockholm University, Stockholm.

Bond, G., Showers, W., Cheseby, M., Lotti, R., Almasi, P., deMenocal, P., Priore, P., Cullen, H., Hajdas, I., Bonani, G., 1997. A Pervasive Millennial-Scale Cycle in North Atlantic Holocene and Glacial Climates. Science 278, 1257–1266. https://doi.org/10.1126/science.278.5341.1257.

ter Braak, C.J.F., Juggins, S., 1993. Weighted averaging partial least squares regression (WA-PLS): An improved method for reconstructing environmental variables from species assemblages. In: van Dam, H. (Ed.), Twelfth International Diatom Symposium. Springer, Netherlands, Dordrecht, pp. 485–502.

Breiman, L., 2001. Random Forests. Mach. Learn. 45, 5–32. https://doi.org/10.1023/A:1010933404324.

Brown, T., Rijal, D.P., Heintzman, P.D., Clarke, C.L., Blankholm, H.P., Høeg, H.I., Lammers, Y., Bråthen, K.A., Edwards, M., Alsos, I.G., 2022. Paleoeconomy more than demography determined prehistoric human impact in Arctic Norway. PNAS Nexus 1, pgac209. https://doi.org/10.1093/pnasnexus/pgac209.

Burczyk, J., Sandurska, E., Lewandowski, A., 2019. Patterns of effective pollen dispersal in larch: linking levels of background pollination with Pollen Dispersal Kernels. Forests 10, 1139. https://doi.org/10.3390/f10121139.

Chevalier, M., Davis, B.A.S., Heiri, O., Seppä, H., Chase, B.M., Gajewski, K., Lacourse, T., Telford, R.J., Finsinger, W., Guiot, J., Kühl, N., Maezumi, S.Y., Tipton, J.R., Carter, V.A., Brussel, T., Phelps, L.N., Dawson, A., Zanon, M., Vallé, F., Nolan, C., Mauri, A., de Vernal, A., Izumi, K., Holmström, L., Marsicek, J., Goring, S., Sommer, P.S., Chaput, M., Kupriyanov, D., 2020. Pollen-based climate reconstruction techniques for late Quaternary studies. Earth Sci. Rev. 210, 103384 https://doi.org/10.1016/j.earscirev.2020.103384.

Clark, P.U., Marshall, S.J., Clarke, G.K.C., Hostetler, S.W., Licciardi, J.M., Teller, J.T., 2001. Freshwater forcing of abrupt climate change during the Last Glaciation. Science 293, 283–287. https://doi.org/10.1126/science.1062517.

Clarke, C.L., Alsos, I.G., Edwards, M.E., Paus, A., Gielly, L., Haflidason, H., Mangerud, J., Regnéll, C., Hughes, P.D.M., Svendsen, J.I., Bjune, A.E., 2020. A 24,000-year ancient DNA and pollen record from the Polar Urals reveals temporal dynamics of arctic and boreal plant communities. Quat. Sci. Rev. 247, 106564 https://doi.org/10.1016/j.quascirev.2020.106564.

Clayden, S.L., Cwynar, L.C., MacDonald, G.M., 1996. Stomate and pollen content of lake surface sediments from across the tree line on the Taimyr Peninsula, Siberia. Can. J. Bot. 74, 1009–1015. https://doi.org/10.1139/b96-125.

Correa-Metrio, A., Dechnik, Y., Lozano-García, S., Caballero, M., 2014. Detrended correspondence analysis: a useful tool to quantify ecological changes from fossil data sets. Bol. Soc. Geol. Mex. 66, 135–143.

Davis, B.A.S., Brewer, S., Stevenson, A.C., Guiot, J., 2003. The temperature of Europe during the Holocene reconstructed from pollen data. Quat. Sci. Rev. 22, 1701–1716. https://doi.org/10.1016/S0277-3791(03)00173-2.

De'ath, G., 2007. Boosted trees for ecological modeling and prediction. Ecology 88, 243–251. https://doi.org/10.1890/0012-9658(2007)88[243:BTFEMA]2.0.CO;2.

Demidov, I.N., Lavrova, N.B., 2001. Quaternary Cover Structure in the Vodla River Basin, Eastern Karelia, and the Late and Post-Glacial Evolution of Vegetation, in: Vodlozero National Park: Wildlife Diversity and Cultural Heritage. Karelian Research Centre, Russian Academy of Sciences, Petrozavodsk, pp. 49–60 (In Russian).

Denton, G.H., Alley, R.B., Comer, G.C., Broecker, W.S., 2005. The role of seasonality in abrupt climate change. Quat. Sci. Rev. 24, 1159–1182. https://doi.org/10.1016/j.quascirev.2004.12.002.

Drobyshev, I., Bergeron, Y., Vernal, A.D., Moberg, A., Ali, A.A., Niklasson, M., 2016. Atlantic SSTs control regime shifts in forest fire activity of Northern Scandinavia. Sci. Rep. 6, 22532 https://doi.org/10.1038/srep22532.

Elmendorf, S.C., Henry, G.H.R., Hollister, R.D., Björk, R.G., Boulanger-Lapointe, N., Cooper, E.J., Cornelissen, J.H.C., Day, T.A., Dorrepaal, E., Elumeeva, T.G., Gill, M., Gould, W.A., Harte, J., Hik, D.S., Hofgaard, A., Johnson, D.R., Johnstone, J.F., Jónsdóttir, I.S., Jorgenson, J.C., Klanderud, K., Klein, J.A., Koh, S., Kudo, G., Lara, M., Lévesque, E., Magnússon, B., May, J.L., Mercado-Dı'az, J.A., Michelsen, A., Molau, U., Myers-Smith, I.H., Oberbauer, S.F., Onipchenko, V.G., Rixen, C., Martin Schmidt, N., Shaver, G.R., Spasojevic, M.J., Þórhallsdóttir, Þ.E., Tolvanen, A., Troxler, T., Tweedie, C.E., Villareal, S., Wahren, C.-H., Walker, X., Webber, P.J., Welker, J.M., Wipf, S., 2012. Plot-scale evidence of tundra vegetation change and links to recent summer warming. Nat. Clim. Chang. 2, 453–457. https://doi.org/10.1038/nclimate1465.

Filimonova, L.V., 2006. Detailed Reconstruction of Paleovegetion of Poorly Studied Areas in Northern and Middle Taiga of Eastern Fennoscandia, in: Structure and Dynamics of Wetland and Grassland Ecosystems of Eastern Fennoscandia. Karelian Research Centre, Russian Academy of Sciences, Petrozavodsk, pp. 129–161 (In Russian).

Forsström, L., 1990. Occurrence of larch (Larix) in Fennoscandia during the Eemian interglacial and the Brørup interstadial according to pollen analytical data. Boreas 19, 241–248. https://doi.org/10.1111/j.1502-3885.1990.tb00449.x.

Garcés-Pastor, S., Coissac, E., Lavergne, S., Schwörer, C., Theurillat, J.-P., Heintzman, P. D., Wangensteen, O.S., Tinner, W., Rey, F., Heer, M., Rutzer, A., Walsh, K., Lammers, Y., Brown, A.G., Goslar, T., Rijal, D.P., Karger, D.N., Pellissier, L., Pouchon, C., Roquet, C., Thuiller, W., Zimmermann, N.E., Alberti, A., Wincker, P., Boleda, M., Boyer, F., Hombiat, A., Perrier, C., Douzet, R., Valay, J.-G., Aubert, S., Denoeud, F., Bzeznick, B., Gielly, L., Taberlet, P., Rioux, D., Orvain, C., Rome, M., Wüest, R.O., Latzin, S., Spillmann, J., Feichtinger, L., Van Es, J., Garraud, L., Villaret, J.-C., Abdulhak, S., Bonnet, V., Huc, S., Fort, N., Legland, T., Sanz, T., Pache, G., Mikolajczak, A., Noble, V., Michaud, H., Offerhaus, B., Dentant, C., Salomez, P., Bonet, R., Delahaye, T., Leccia, M.-F., Perfus, M., Eggenberg, S., Möhl, A., Hurdu, B.-I., Szatmari, P.-M., Puşcaş, M., Smyčka, J., Mráz, P., Šemberová, K., Ronikier, M., Slovák, M., Heiri, O., Alsos, I.G., The PhyloAlps, C., 2022. High resolution ancient sedimentary DNA shows that alpine plant diversity is associated with human land use and climate change. Nat. Commun. 13, 6559 https://doi.org/10.1038/s41467-022-34010-4.

van Geel, B., 2001. Non-pollen palynomorphs. In: Smol, J.P., Birks, H.J.B., Last, W.M. (Eds.), Tracking Environmental Change Using Lake Sediments. Volume 3: Terrestrial, Algal, and Siliceous Indicators. Kluwer Academic Publishers, Dordrecht, pp. 99–119.

Gower, S.T., Richards, J.H., 1990. Larches: deciduous conifers in an evergreen world. BioScience 40, 818–826. https://doi.org/10.2307/1311484.

Grimm, E., 1987. CONISS: a FORTRAN 77 program for stratigraphically constrained cluster analysis by the method of incremental sum of squares. Comput. Geosci. 13, 13–35. https://doi.org/10.1016/0098-3004(87)90022-7.

He, F., Shakun, J.D., Clark, P.U., Carlson, A.E., Liu, Z., Otto-Bliesner, B.L., Kutzbach, J.E., 2013. Northern Hemisphere forcing of Southern Hemisphere climate during the last deglaciation. Nature 494, 81–85. https://doi.org/10.1038/nature11822.

Heikkilä, M., Seppä, H., 2003. A 11,000 yr palaeotemperature reconstruction from the southern boreal zone in Finland. Quat. Sci. Rev. 22, 541–554. https://doi.org/10.1016/S0277-3791(02)00189-0.

Helmens, K.F., Väliranta, M., Engels, S., Shala, S., 2012. Large shifts in vegetation and climate during the early Weichselian (MIS 5d-c) inferred from multi-proxy evidence at Sokli (northern Finland). Quat. Sci. Rev. 41, 22–38. https://doi.org/10.1016/j.quascirev.2012.02.008.

Helmens, K.F., Katrantsiotis, C., Kuosmanen, N., Luoto, T.P., Salonen, J.S., Väliranta, M., 2021. Prolonged interglacial warmth during the Last Glacial in northern Europe. Boreas 50, 331–350. https://doi.org/10.1111/bor.12495.

Herrle, J.O., Bollmann, J., Gebühr, C., Schulz, H., Sheward, R.M., Giesenberg, A., 2018. Black Sea outflow response to Holocene meltwater events. Sci. Rep. 8, 4081. https://doi.org/10.1038/s41598-018-22453-z.

Jankovská, V., Andreev, A.A., Panova, N.K., 2006. Holocene environmental history on the eastern slope of the Polar Ural Mountains, Russia. Boreas 35, 650–661. https://doi.org/10.1111/j.1502-3885.2006.tb01171.x.

Johansson, P., 1995. The Deglaciation in the Eastern Part of the Weichselian Ice Divide in Finnish Lapland. Geological Survey of Finland, Rovaniemi.

Johansson, P., 2007. Late Weichselian deglaciation in Finnish Lapland. In: Johansson, P., Sarala, P. (Eds.), Applied Quaternary Research in the Central Part of Glaciated Terrain. Geological Survey of Finland, Espoo, pp. 47–54.

Jokinen, P., Pirinen, P., Kaukoranta, J.P., Kangas, A., Alenius, P., Eriksson, P., Johansson, M., Wilkman, S., 2021. Climatological and oceanographic statistics of Finland 1991–2020. Reports 2021. Finnish Meteorological Institute, Helsinki.

Juggins, S., 2013. Quantitative reconstructions in palaeolimnology: new paradigm or sick science? Quat. Sci. Rev. 64, 20–32. https://doi.org/10.1016/j.quascirev.2012.12.014.

Juggins, S., 2020. rioja: Analysis of Quaternary Science Data, R package version 0.8-7. http://CRAN.R-project.org/package=rioja (accessed 30 April 2024).

Kanerva, R., 1956. Pollenanalytische Studien über die spätquartäre Wald- und Klimageschichte von Hyrynsalmi in NO-Finnland. The Finnish Academy of Science and Letters, Helsinki (In German).

Karger, D.N., Nobis, M.P., Normand, S., Graham, C.H., Zimmermann, N.E., 2023. CHELSA-TraCE21k – high-resolution (1 km) downscaled transient temperature and precipitation data since the Last Glacial Maximum. Clim. Past 19, 439–456. https://doi.org/10.5194/cp-19-439-2023.

Kaufman, D., McKay, N., Routson, C., Erb, M., Davis, B., Heiri, O., Jaccard, S., Tierney, J., Dätwyler, C., Axford, Y., Brussel, T., Cartapanis, O., Chase, B., Dawson, A., de Vernal, A., Engels, S., Jonkers, L., Marsicek, J., Moffa-Sánchez, P., Morrill, C., Orsi, A., Rehfeld, K., Saunders, K., Sommer, P.S., Thomas, E., Tonello, M., Tóth, M., Vachula, R., Andreev, A., Bertrand, S., Biskaborn, B., Bringué, M., Brooks, S., Caniupán, M., Chevalier, M., Cwynar, L., Emile-Geay, J., Fegyveresi, J., Feurdean, A., Finsinger, W., Fortin, M.-C., Foster, L., Fox, M., Gajewski, K., Grosjean, M., Hausmann, S., Heinrichs, M., Holmes, N., Ilyashuk, B., Ilyashuk, E., Juggins, S., Khider, D., Koinig, K., Langdon, P., Larocque-Tobler, I., Li, J., Lotter, A., Luoto, T., Mackay, A., Magyari, E., Malevich, S., Mark, B., Massaferro, J., Montade, V., Nazarova, L., Novenko, E., Pařil, P., Pearson, E., Peros, M., Pienitz, R., Płóciennik, M., Porinchu, D., Potito, A., Rees, A., Reinemann, S., Roberts, S., Rolland, N., Salonen, S., Self, A., Seppä, H., Shala, S., St-Jacques, J.-M., Stenni, B., Syrykh, L., Tarrats, P., Taylor, K., van den Bos, V., Velle, G., Wahl, E., Walker, I., Wilmshurst, J., Zhang, E., Zhilich, S., 2020a. A global database of Holocene paleotemperature records. Sci. Data 7, 115. https://doi.org/10.1038/s41597-020-0445-3.

Kaufman, D., McKay, N., Routson, C., Erb, M., Dätwyler, C., Sommer, P.S., Heiri, O., Davis, B., 2020b. Holocene global mean surface temperature, a multi-method reconstruction approach. Sci. Data 7, 201. https://doi.org/10.1038/s41597-020-0530-7.

Kharuk, V., Ranson, K., Dvinskaya, M., 2007. Evidence of Evergreen Conifer Invasion into Larch Dominated Forests during recent decades in Central Siberia. Eurasian J. For. Res. 10, 163–171.

Kuang, X., Schenk, F., Smittenberg, R., Hällberg, P., Zhang, Q., 2021. Seasonal evolution differences of east Asian summer monsoon precipitation between Bølling-Allerød and younger Dryas periods. Clim. Chang. 165, 19. https://doi.org/10.1007/s10584-021-03025-z.

Kuhry, P., 1997. The palaeoecology of a treed bog in western boreal Canada: a study based on microfossils, macrofossils and physico-chemical properties. Rev. Palaeobot. Palynol. 96, 183–224. https://doi.org/10.1016/S0034-6667(96)00018-8.

Kullman, L., 1998. Palaeoecological, biogeographical and palaeoclimatological implications of early Holocene Immigration of Larix sibirica Ledeb. Into the Scandes Mountains, Sweden. Glob. Ecol. Biogeogr. Lett. 7, 181–188. https://doi.org/10.2307/2997373.

Kultti, S., Väliranta, M., Sarmaja-Korjonen, K., Solovieva, N., Virtanen, T., Kauppila, T., Eronen, M., 2003. Palaeoecological evidence of changes in vegetation and climate during the Holocene in the pre-Polar Urals, northeast European Russia. J. Quat. Sci. 18, 503–520. https://doi.org/10.1002/jqs.765.

Kuosmanen, N., Fang, K., Bradshaw, R.H., Clear, J.L., Seppä, H., 2014. Role of forest fires in Holocene stand-scale dynamics in the unmanaged taiga forest of northwestern Russia. Holocene 24, 1503–1514. https://doi.org/10.1177/0959683614544065.

Kuosmanen, N., Seppä, H., Reitalu, T., Alenius, T., Bradshaw, R.H.W., Clear, J.L., Filimonova, L., Kuznetsov, O., Zaretskaya, N., 2016. Long-term forest composition and its drivers in taiga forest in NW Russia. Veg. Hist. Archaeobotany 25, 221–236. https://doi.org/10.1007/s00334-015-0542-y.

Lampinen, R., Lahti, T., 2023. Kasviatlas. Finnish Museum of Natural History. University of Helsinki. https://kasviatlas.fi/ (accessed 30 April 2024. In Finnish).

Leitner, R., Gajewski, K., 2004. Modern and Holocene stomate records of tree-line variations in northwestern Quebec. Can. J. Bot. 82, 726–734. https://doi.org/10.1139/b04-050.

Li, M., Wang, F., Cai, B., Cao, Q., Cheng, H., Shen, C.-C., Tan, M., Edwards, R.L., 2022. Timing and Structure of 10.9 and 10.3 ka BP events Revealed by Annually Laminated Stalagmite Records from Shihua Cave, Northern China. Paleoceanogr. Paleoclimatol. 37, e2022PA004459 https://doi.org/10.1029/2022PA004459.

Liaw, A., Wiener, M., 2002. Classification and Regression by randomForest. R News 2/3, pp. 18–22.

Liu, Z., Otto-Bliesner, B.L., He, F., Brady, E.C., Tomas, R., Clark, P.U., Carlson, A.E., Lynch-Stieglitz, J., Curry, W., Brook, E., Erickson, D., Jacob, R., Kutzbach, J., Cheng, J., 2009. Transient simulation of Last Deglaciation with a new mechanism for Bølling-Allerød warming. Science 325, 310–314. https://doi.org/10.1126/science.1171041.

Maher, L.J., 1972. Nomograms for computing 0.95 confidence limits of pollen data. Rev. Palaeobot. Palynol. 13, 85–93. https://doi.org/10.1016/0034-6667(72)90038-3.

Mäkelä, E., Sarmaja-Korjonen, K., Hyvärinen, H., 1994. Holocene forest history of the Pöyrisjärvi area north of the coniferous tree line in western Finnish Lapland: a pollen stratigraphical study. B. Geol. Soc. Finl. 66, 81–94. https://doi.org/10.17741/bgsf/66.2.003.

Mauquoy, D., van Geel, B., 2013. Mire and Peat Macros. In: Elias, S.A., Mock, C.J. (Eds.), Encyclopedia of Quaternary Science, Second edition. Elsevier, Amsterdam, pp. 637–656.

Moore, P.D., Webb, J.A., Collison, M., 1991. Pollen Analysis, Second ed. Blackwell Scientific Publications, London.

Öberg, L., Kullman, L., 2011. Ancient Subalpine Clonal Spruces (Picea abies): sources of postglacial vegetation history in the Swedish Scandes. Arctic 64, 183–196.

Oksanen, J., 2022. vegan: Community Ecology Package, R package version 2.6–4. https://CRAN.R-project.org/package=vegan.

Overpeck, J.T., Webb III, T., Prentice, I.C., 1985. Quantitative interpretation of fossil pollen spectra: dissimilarity coefficients and the method of modern analogs. Quat. Res. 23, 87–108. https://doi.org/10.1016/0033-5894(85)90074-2.

Plikk, A., Helmens, K.F., Fernández-Fernández, M., Kylander, M., Löwemark, L., Risberg, J., Salonen, J.S., Väliranta, M., Weckström, J., 2016. Development of an Eemian (MIS 5e) Interglacial palaeolake at Sokli (N Finland) inferred using multiple

proxies. Palaeogeogr. Palaeoclimatol. Palaeoecol. 463, 11–26. https://doi.org/10.1016/j.palaeo.2016.09.008.
Putkinen, S., Saarelainen, J., 1998. Kullenbergin näytteenottimen uusi kevennetty malli. Geologi 50, 22–23 (In Finnish).
R Core Team, 2022. R: A Language and Environment for Statistical Computing. R Foundation for Statistical Computing, Vienna. https://www.R-project.org/ (accessed 30 April 2024).
Rasmussen, S.O., Vinther, B.M., Clausen, H.B., Andersen, K.K., 2007. Early Holocene climate oscillations recorded in three Greenland ice cores. Quat. Sci. Rev. 26, 1907–1914. https://doi.org/10.1016/j.quascirev.2007.06.015.
Reille, M., 1992. Pollen et Spores d'Europe et d'Afrique du Nord. Laboratoire de Botanique Historique et Palynologie, URA CNRS, Marseille.
Renssen, H., Seppä, H., Crosta, X., Goosse, H., Roche, D.M., 2012. Global characterization of the Holocene thermal Maximum. Quat. Sci. Rev. 48, 7–19. https://doi.org/10.1016/j.quascirev.2012.05.022.
Renssen, H., Goosse, H., Roche, D.M., Seppä, H., 2018. The global hydroclimate response during the Younger Dryas event. Quat. Sci. Rev. 193, 84–97. https://doi.org/10.1016/j.quascirev.2018.05.033.
Revéret, A., Rijal, D.P., Heintzman, P.D., Brown, A.G., Stoof-Leichsenring, K.R., Alsos, I. G., 2023. Environmental DNA of aquatic macrophytes: The potential for reconstructing past and present vegetation and environments. Freshw. Biol. 68, 1929–1950. https://doi.org/10.1111/fwb.14158.
Ridgeway, G., 2020. gbm: Generalized Boosted Regression Models, R package version 2.1.8. http://CRAN.R-project.org/package=gbm (accessed 30 April 2024).
Rijal, D.P., Heintzman, P.D., Lammers, Y., Yoccoz, N.G., Lorberau, K.E., Pitelkova, I., Goslar, T., Murguzur, F.J.A., Salonen, J.S., Helmens, K.F., Bakke, J., Edwards, M.E., Alm, T., Bråthen, K.A., Brown, A.G., Alsos, I.G., 2021. Sedimentary ancient DNA shows terrestrial plant richness continuously increased over the Holocene in northern Fennoscandia. Sci. Adv. 7, eabf9557 https://doi.org/10.1126/sciadv.abf9557.
Salonen, J.S., Seppä, H., Luoto, M., Bjune, A.E., Birks, H.J.B., 2012. A north European pollen–climate calibration set: analysing the climatic responses of a biological proxy using novel regression tree methods. Quat. Sci. Rev. 45, 95–110. https://doi.org/10.1016/j.quascirev.2012.05.003.
Salonen, J.S., Helmens, K.F., Seppä, H., Birks, H.J.B., 2013. Pollen-based palaeoclimate reconstructions over long glacial-interglacial timescales: methodological tests based on the Holocene and MIS 5d-c deposits at Sokli, northern Finland. J. Quat. Sci. 28, 271–282. https://doi.org/10.1002/jqs.2611.
Salonen, J.S., Luoto, M., Alenius, T., Heikkilä, M., Seppä, H., Telford, R.J., Birks, H.J.B., 2014. Reconstructing palaeoclimatic variables from fossil pollen using boosted regression trees: comparison and synthesis with other quantitative reconstruction methods. Quat. Sci. Rev. 88, 69–81. https://doi.org/10.1016/j.quascirev.2014.01.011.
Salonen, J.S., Helmens, K.F., Brendryen, J., Kuosmanen, N., Valiranta, M., Goring, S., Korpela, M., Kylander, M., Philip, A., Plikk, A., Renssen, H., Luoto, M., 2018. Abrupt high-latitude climate events and decoupled seasonal trends during the Eemian. Nat. Commun. 9, 2851. https://doi.org/10.1038/s41467-018-05314-1.
Salonen, J.S., Korpela, M., Williams, J.W., Luoto, M., 2019. Machine-learning based reconstructions of primary and secondary climate variables from north American and European fossil pollen data. Sci. Rep. 9, 15805. https://doi.org/10.1038/s41598-019-52293-4.
Salonen, J.S., Sánchez-Goñi, M.F., Renssen, H., Plikk, A., 2021. Contrasting northern and southern European winter climate trends during the Last Interglacial. Geology 49, 1220–1224. https://doi.org/10.1130/G49007.1.
Sarmaja-Korjonen, K., Seppä, H., 2007. Abrupt and consistent responses of aquatic and terrestrial ecosystems to the 8200 cal. Yr cold event: a lacustrine record from Lake Arapisto, Finland. Holocene 17, 457–467. https://doi.org/10.1177/0959683607077020.
Schenk, F., Wohlfarth, B., 2019. The Imprint of Hemispheric-Scale Climate Transitions on the European Climate during the Last Deglaciation (15.5 Ka to 9 Ka BP). SKB Technical Report.
Schenk, F., Väliranta, M., Muschitiello, F., Tarasov, L., Heikkilä, M., Björck, S., Brandefelt, J., Johansson, A.V., Näslund, J.-O., Wohlfarth, B., 2018. Warm summers during the Younger Dryas cold reversal. Nat. Commun. 9, 1634. https://doi.org/10.1038/s41467-018-04071-5.
Seppä, H., Birks, H.H., Birks, H.J.B., 2002. Rapid climatic changes during the Greenland stadial 1 (Younger Dryas) to early Holocene transition on the Norwegian Barents Sea coast. Boreas 31, 215–225. https://doi.org/10.1111/j.1502-3885.2002.tb01068.x.
Seppä, H., Birks, H.J.B., Giesecke, T., Hammarlund, D., Alenius, T., Antonsson, K., Bjune, A.E., Heikkilä, M., MacDonald, G.M., Ojala, A.E.K., Telford, R.J., Veski, S., 2007. Spatial structure of the 8200 cal yr BP event in northern Europe. Clim. Past 3, 225–236. https://doi.org/10.5194/cp-3-225-2007.
Seppä, H., Alenius, T., Bradshaw, R.H.W., Giesecke, T., Heikkilä, M., Muukkonen, P., 2009a. Invasion of Norway spruce (Picea abies) and the rise of the boreal ecosystem in Fennoscandia. J. Ecol. 97, 629–640. https://doi.org/10.1111/j.1365-2745.2009.01505.x.
Seppä, H., Bjune, A.E., Telford, R.J., Birks, H.J.B., Veski, S., 2009b. Last nine-thousand years of temperature variability in Northern Europe. Clim. Past 5, 523–535. https://doi.org/10.5194/cp-5-523-2009.
Shala, S., Helmens, K.F., Jansson, K.N., Kylander, M.E., Risberg, J., Löwemark, L., 2014. Palaeoenvironmental record of glacial lake evolution during the early Holocene at Sokli, NE Finland. Boreas 43, 362–376. https://doi.org/10.1111/bor.12043.
Shala, S., Helmens, K.F., Luoto, T.P., Salonen, J.S., Väliranta, M., Weckström, J., 2017. Comparison of quantitative Holocene temperature reconstructions using multiple proxies from a northern boreal lake. Holocene 27, 1745–1755. https://doi.org/10.1177/0959683617708442.
Shuman, J.K., Shugart, H.H., O'Halloran, T.L., 2011. Sensitivity of Siberian larch forests to climate change. Glob. Chang. Biol. 17, 2370–2384. https://doi.org/10.1111/j.1365-2486.2011.02417.x.
Sjögren, P., Edwards, M.E., Gielly, L., Langdon, C.T., Croudace, I.W., Merkel, M.K.F., Fonville, T., Alsos, I.G., 2017. Lake sedimentary DNA accurately records 20th Century introductions of exotic conifers in Scotland. New Phytol. 213, 929–941. https://doi.org/10.1111/nph.14199.
Stockmarr, J., 1971. Tables with spores used in absolute pollen analysis. Pollen Spores 13, 615–621.
Subetto, D.A., Wohlfarth, B., Davydova, N.N., Sapelko, T.V., Björkman, L., Solovieva, N., Wastegård, S., Possnert, G., Khomutova, V.I., 2002. Climate and environment on the Karelian Isthmus, northwestern Russia, 13000-9000 cal. Yrs BP. Boreas 31, 1–19. https://doi.org/10.1111/j.1502-3885.2002.tb01051.x.
Sundqvist, H.S., Zhang, Q., Moberg, A., Holmgren, K., Körnich, H., Nilsson, J., Brattström, G., 2010. Climate change between the mid and late Holocene in northern high latitudes – part 1: survey of temperature and precipitation proxy data. Clim. Past 6, 591–608. https://doi.org/10.5194/cp-6-591-2010.
Sweeney, C.A., 2004. A key for the identification of stomata of the native conifers of Scandinavia. Rev. Palaeobot. Palynol. 128, 281–290. https://doi.org/10.1016/S0034-6667(03)00138-6.
Tallavaara, M., Manninen, M.A., Pesonen, P., Hertell, E., 2014. Radiocarbon dates and postglacial colonisation dynamics in eastern Fennoscandia. In: Riede, F., Tallavaara, M. (Eds.), Lateglacial and Postglacial Pioneers in Northern Europe. Archaeopress, Oxford, pp. 161–175.
Thomas, P.A., El-Barghathi, M., Polwart, A., 2007. Biological Flora of the British Isles: Juniperus communis L. J. Ecol. 95, 1404–1440. https://doi.org/10.1111/j.1365-2745.2007.01308.x.
Tyler, T., Herbertsson, L., Olofsson, J., Olsson, P.A., 2021. Ecological indicator and traits values for Swedish vascular plants. Ecol. Indic. 120, 106923 https://doi.org/10.1016/j.ecolind.2020.106923.
Väliranta, M., Salonen, J.S., Heikkilä, M., Amon, L., Helmens, K., Klimaschewski, A., Kuhry, P., Kultti, S., Poska, A., Shala, S., Veski, S., Birks, H.H., 2015. Plant macrofossil evidence for an early onset of the Holocene summer thermal maximum in northernmost Europe. Nat. Commun. 6, 6809. https://doi.org/10.1038/ncomms7809.
Van Der Wiel, A.M., 1982. A palaeoecological study of a section from the foot of the Hazendonk (Zuid-Holland, The Netherlands), based on the analysis of pollen, spores and macroscopic plant remains. Rev. Palaeobot. Palynol. 38, 35–90. https://doi.org/10.1016/0034-6667(82)90049-5.
Van Geel, B., Hallewas, D.P., Pals, J.P., 1983. A late holocene deposit under the Westfriese Zeedijk near Enkhuizen (Prov. Of Noord-Holland, The Netherlands): Palaeoecological and archaeological aspects. Rev. Palaeobot. Palynol. 38, 269–335. https://doi.org/10.1016/0034-6667(83)90026-X.
Van Geel, B., Coope, G.R., Van Der Hammen, T., 1989. Palaeoecology and stratigraphy of the lateglacial type section at Usselo (the Netherlands). Rev. Palaeobot. Palynol. 60, 25–129. https://doi.org/10.1016/0034-6667(89)90072-9.
Vasari, Y., 1962. A study of the vegetational history of the Kuusamo district (Northeast Finland) during the late-Quaternary period. Ann. Bot. Soc. Zool. Bot. Fenn. Vanamo 33, 1–138.
Venäläinen, A., Tuomenvirta, H., Pirinen, P., Drebs, A., 2005. A Basic Climate Data Set 1961–2000—Description and Illustrations. Reports 0782-6079.. Finnish Meteorological Institute, Helsinki.
Veski, S., Seppä, H., Ojala, A.E.K., 2004. Cold event at 8200 yr B.P. Recorded in annually laminated lake sediments in eastern Europe. Geology 32, 681–684. https://doi.org/10.1130/G20683.1.
Virtanen, T., Neuvonen, S., Nikula, A., 1998. Modelling topoclimatic patterns of egg mortality of Epirrita autumnata (Lepidoptera: Geometridae) with a Geographical Information System: predictions for current climate and warmer climate scenarios. J. Appl. Ecol. 35, 311–322. https://doi.org/10.1046/j.1365-2664.1998.00299.x.